RESEARCH ARTICLE

Satellite Swarm-Based Antenna Arrays for 6G Direct-to-Cell Connectivity

DIEGO TUZI, (Graduate Student Member, IEEE), **THOMAS DELAMOTTE**, (Member, IEEE), **AND ANDREAS KNOPP**, (Senior Member, IEEE)

Institute of Information Technology, University of the Bundeswehr Munich, 85579 Neubiberg, Germany

Corresponding author: Diego Tuzi (paper.sp@unibw.de)

ABSTRACT Direct connectivity in L/S frequency bands between satellites and common mobile terrestrial user equipment (UE), such as smartphones, is an essential feature for future 6G non-terrestrial networks. The technical trend in closing the link between the communication endpoints is to develop large phased antenna arrays to be launched in LEO orbit. Satellite swarms represent an innovative and promising approach. Swarms are composed of several small and lightweight satellites organized in a free-flying formation (i.e., wireless connected) or a tethered formation (i.e., wired connected) creating a distributed phased antenna array. It has the potential to provide an enhanced gain, narrower beam width and lower launch/build costs compared to conventional single satellite systems with large phased antenna arrays. The first objective of this work is the design of swarm-based antenna arrays, in which the impact of key parameters such as the number of satellites in the swarm, their reciprocal distance and the array geometry, is thoroughly analyzed. It is shown that the undesired phenomenon of grating lobes can be mitigated via optimized array geometries and a new geometry named the enhanced logarithmic spiral array (ELSA) is presented. The second objective of this work is the identification of the most important research directions and system design aspects for the swarm system. In particular, it is shown that tethered swarms with ELSA geometries, innovative deployable structures and very small satellites can foster the deployment of swarms in future satellite systems.

INDEX TERMS 6G, CubeSats, direct-to-cell, distributed satellite systems, ELSA, free-flying formation, grating lobes, NTN, satellite swarm, tethered formation.

I. INTRODUCTION

The direct connectivity between satellites and common mobile terrestrial user equipment (UE), e.g., smartphones, currently referred to with different terms, such as direct satellite-to-device, direct satellite-to-phone, direct satellite-to-handset, direct satellite-to-handheld or simply direct-to-cell connectivity, represents an attractive and essential feature for future non-terrestrial networks. Satellite systems could access billions of mobile subscribers through direct connectivity. This immense potential fosters a huge interest in the industry. An increasing number of companies are working on direct connectivity, offering basic emergency services using existing constellations, such as Apple [1] and Huawei [2] or planning and testing new solutions, such as Lynk [3]. Although these examples represent the first commercial services between satellites and common terrestrial UEs, they rely on a very limited exchange of data that is not suitable for services offered in terrestrial networks. To provide higher performance, several difficulties must be addressed. The main difficulties are related to the distance between the endpoints and the low antenna gain of the UE, therefore, new degrees of freedom should be explored to improve the link budget. The UE can only have little performance improvements for several reasons (a bulky external antenna is not an option). Current systems have been considering low Earth orbits (LEO) and lower frequency bands (L, S bands) to reduce the channel impairments such as free space path loss and

The associate editor coordinating the review of this manuscript and approving it for publication was Hassan Tariq Chattha.
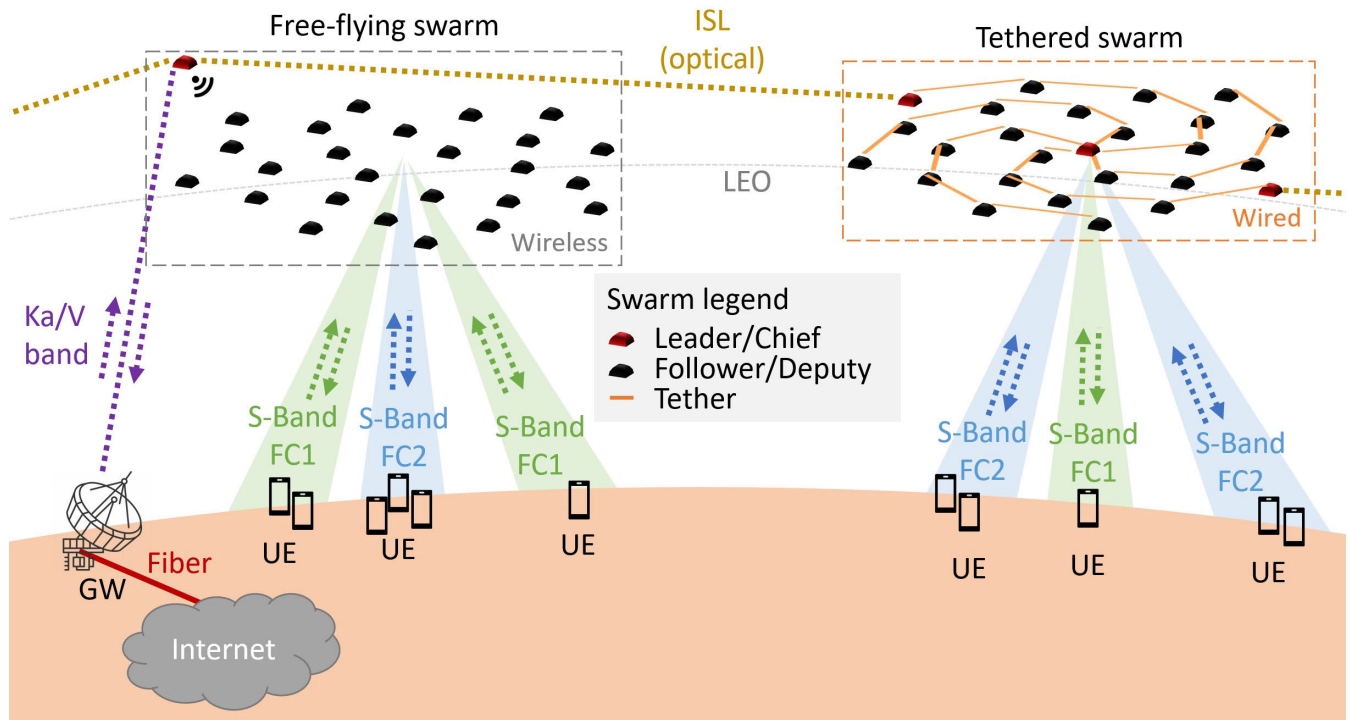
FIGURE 1. Example operative scenario with free-flying and tethered swarms.

atmospheric attenuation, but it is not enough to meet the objective. When conventional single satellite communication systems are considered, the link budget in a direct connectivity scenario can only be closed if the payload is also equipped with a sufficiently large antenna reflector and/or the power is increased. In the literature and on the market, there are new mechanical solutions to create large spaceborne deployable satellite antennas which are easier to launch with rockets. These structures are large antenna reflectors folded on Earth and able to unfold in space. The book in [4] reports the current status and the research directions in the field of large deployable satellite antennas while in [5] there is an example of a commercially available product. Better flexibility on the satellite side can be achieved thanks to large phased antenna arrays. As an example, SpaceX and T-Mobile have recently announced a joint plan called ''Coverage Above and Beyond'' and according to [6], the new SpaceX satellites might use an antenna array with side dimensions of 5m. Another important example, that combines the benefits of a large phased array and a deployable structure, is the test satellite BlueWalker 3 developed by AST SpaceMobile [7]. This is a massive satellite, with a surface of $64m^2$, but according to the plan of the company, the future constellation will be based on larger BlueBird satellites [8]. Furthermore, the same company wrote the patent in [9] envisioning the use of a distributed architecture for direct connectivity. Although these examples show the industry's interest in direct-to-cell connectivity, they also evidence the increment of costs and difficulties to build and launch the satellites.

In this dynamic context, this paper introduces the ''Satellite Swarm'' architecture (from now on referred to as ''swarm''). The swarm represents an innovative and promising solution to the direct-to-cell connectivity use case. It is a distributed system composed of several small and lightweight satellites, e.g., CubeSats, equipped with a commercial low gain patch antenna. It is tuned to create a large equivalent aperture providing a huge gain and a narrow beam. The swarm elements can be arranged in a free-flying configuration (i.e., wireless connected) or tethered configuration (i.e., wired connected) as the operative example illustrated in Fig. 1. It usually has one or more satellites with enhanced capabilities, called leader/s or chief/s while the other satellites of the formation are called followers or deputies. The leader can be part of the swarm or an external satellite outside the formation. Different implementations are possible depending on how the tasks are distributed among leader/s and followers. In one possible implementation, the leader distributes the signal to the followers. The followers transmit a phase-shifted version of the same signal to achieve a coherent sum of the signals in the desired beam direction.

Swarms appear as a promising flexible solution to reduce the design and launch costs of satellite systems for direct connectivity [10]. A system cost analysis for the specific case of a space telescope shows that swarm configurations are more cost-effective than a monolithic approach [11]. In addition to the cost reduction, the distributed nature of the swarm provides several additional benefits. Firstly, the workload distribution on multiple elements makes the swarm

fault-tolerant, a failure of single or multiple elements in the swarm leads to a graceful performance degradation but not a service interruption. Secondly, the swarm introduces scalability to the system, the performance can be easily improved by adding more elements to the swarm. Swarms are a key enabler to guarantee a cost-efficient realization of high-gain apertures.

The benefits of a distributed approach for direct connectivity are also recognized in the AST SpaceMobile patent from [9]. The patent covers several system aspects ranging from the implementation to the operation, but it underestimates the related challenges. It envisions any suitable size and shape for the distributed array and element spacing, but it does not mention the well-known problem of the grating lobes, which is the main limitation when increasing the element spacing between the elements of the array. Grating lobes are lobes in the array beam pattern having an amount of energy comparable to the main lobe but in unwanted directions. They appear as soon as the spacing between the array elements exceeds half the wavelength ($\lambda/2$). The problem has been studied in the literature [12], [13], [14], [15], [16], [17], but they often consider a huge number of elements and a limited range of element spacing. Accordingly, the first objective of this paper is the geometrical design of the swarm array. This work considers existing solutions for the mitigation of the grating lobes, but an element spacing of up to seven wavelengths has been considered which, according to the authors' knowledge, has not been considered in previous works. In addition, a new geometry, named enhanced logarithmic array (ELSA), based on existing solutions is presented and analyzed.

Although the geometric design of the array is a crucial aspect, it is only one of the challenges related to the swarm system. Therefore, the second objective of this paper is to identify future research directions and important system design aspects. In future research directions, initial considerations are carried out on beamforming optimization, synchronization methods and imperfection analysis. Furthermore, in the system design aspects, several challenges and opportunities for free-flying and tethered swarms are highlighted, such as the importance of the formation flying's stability and the role of innovative deployable structures.

The document then follows this structure:

- Section II presents an overview of the available literature related to swarms;
- Section III discusses the optimization of the swarm-based antenna array geometry;
- Section IV addresses the future research directions related to the communication technology aspects;
- Section V presents related critical system design aspects;
- Section VI summarizes and comments on the main achieved results.

II. STATE-OF-THE-ART REVIEW

The satellite swarm is one of the possible multi-satellite configurations inside the area of distributed satellite systems (DSS). It refers to an architecture with a multitude of identical and autonomous small satellites capable of achieving a common goal with their common behavior. It is also strictly related to other multi-satellite configurations, such as the formation flying and fractionated spacecraft. The term formation flying is usually referred to the problem of keeping a desired relative separation, orientation or position between or among spacecraft. The term fractionated refers to an architecture where a monolithic satellite is decomposed into similar or dissimilar modules with different functions. Although these configurations are different, the needed research can overlap, e.g., a free-flying swarm needs a stable formation flying and the tasks subdivision among leaders and followers is a concept from fractionated spacecraft. A more specific comparison of the DSS terminologies can be found in [18].

Several publications (e.g. [19], [20]) recognize the work in [21], written in 1977, as the first application of the multi-satellite concept to create an interferometric infrared synthetic aperture imaging. Since then, numerous research and space flight demonstrations have been conducted for different fields of application like astronomy, deep-space communications, meteorology, and environmental uses [20]. Most missions have been conducted with a limited number of satellites, but in recent decades research has been considering systems with an increasing number of satellites, especially with the advent of small satellites (e.g., CubeSats and satellites on printed circuit boards or silicon chips) [22], [23], [24]. The work in [11] presents a system architecture considering 100-gram class spacecraft organized in a swarm of 100-1000 elements. An interesting publication realizing synthesis aperture radiometers (SAR) for Earth observation and astronomy purposes is [25]. In this work, a free-flying swarm synthesizing a helix structure and a swarm connected by tethers forming an end-fire array are evaluated. Another example is the recent publication in [26] that considers a simulation with a swarm consisting of up to 96 satellites. Another interesting work on deep-space communication is [27] which shows a distributed swarm array composed of CubeSats able to provide coherent communication in the Ka/X band. Recent publications have studied the use of multi-satellite configurations to provide direct connectivity to Earth, but consider a higher frequency, a smaller number of more powerful satellites [28], [29], [30], and consider more powerful ground terminals. Although not related to the swarm, the work in [31] analyzes the direct connectivity from NGSO Satellites to 5G devices in millimeter waves (28 and 39 GHz).

Despite the efforts invested in the design of swarms for various applications, swarms for direct-to-cell connectivity have until now focused little attention and key challenges remain to be addressed [32]. A recent publication in [33] analyzes multiple satellites equipped with regular planar arrays organized in a square-shaped formation. The study analyzes both GEO and LEO scenarios to provide 5G-like communication services to hand-held user terminals. The authors concluded that the proposed solution is less attractive in the LEO scenario because it does not show a clear benefit
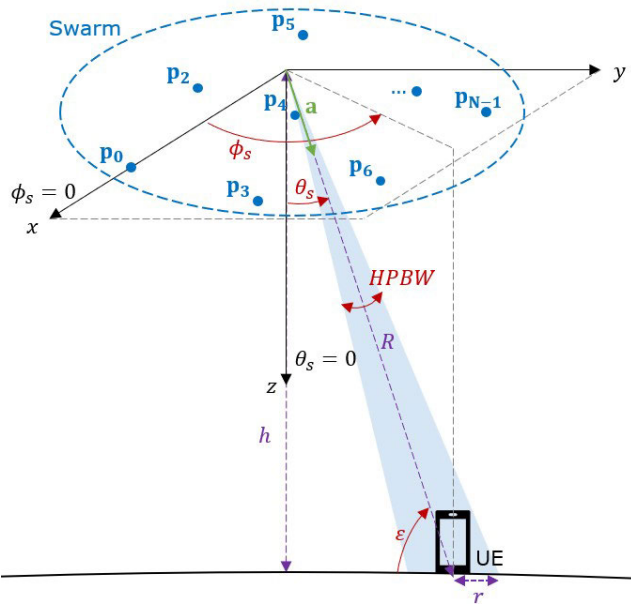
FIGURE 2. Generic scenario representation: Communication endpoints (Swarm and UE) and main parameters (described in Table 1).

compared to the large deployable phased array solution (like the AST SpaceMobile BlueWalker 3). This conclusion does not apply to the general case of multiple satellite systems. Swarms can have great potential in LEO, as will be shown in this paper.

III. SWARM-BASED ANTENNA ARRAY DESIGN

This section presents the first objective of this paper, the design of a swarm-based antenna array. Firstly, it describes the scenario, defines the key performance indicators and identifies the requirements and design goals of the design process. Secondly, it defines the reference architecture based on a planar geometry and shows when the well-known problem of the grating lobes appears. In this context, several details related to BlueWalker 3 are presented because of its similarities with the reference architecture. Thirdly, the paper presents improved architectures for the grating lobes mitigation. Finally, the results of the considered architecture are presented and compared.

A. SCENARIO, KPIs AND DESIGN GOALS DEFINITION
1) SCENARIO DEFINITION

The generic scenario is in Fig. 2. The swarm is represented by N satellites located according to the position vector $\mathbf{p_n}$.

In the proposed scenario, the swarm has to generate one beam in the desired direction, known a priori. In this case, the phase components of the complex weights are derived directly with a geometrical calculation based on the angle of departure (AoD) and the geometry of the swarm.

In addition, antenna losses (e.g., internal dissipation and impedance mismatch caused by mutual coupling between elements) are considered negligible.

a: PHASED ANTENNA ARRAY MODEL

In this context, due to the relatively small distance between the satellites in the swarms compared to the distance between each satellite and the UE, the narrowband model of the phased array presented in the classical array theory in [34] is used to model the swarm. In the general formulation, a phased array can be described through its frequency-wavenumber response function

$$\Upsilon(\omega, \mathbf{k}) = \mathbf{w}^H \mathbf{v}_k(\mathbf{k}), \qquad (1)$$

where the complex weight vector is expressed as

$$\mathbf{w}^H = [w_0^* \, w_1^* \, \cdots \, w_{N-1}^*], \qquad (2)$$

the manifold vector is

$$\mathbf{v}_k(\mathbf{k}) = \begin{bmatrix} e^{-\mathbf{k}^T \mathbf{p}_0} \\ e^{-\mathbf{k}^T \mathbf{p}_1} \\ \vdots \\ e^{-\mathbf{k}^T \mathbf{p}_{N-1}} \end{bmatrix}, \qquad (3)$$

the wavenumber is

$$\mathbf{k} = \frac{2\pi}{\lambda} \mathbf{a}(\theta, \phi), \qquad (4)$$

$\mathbf{a}$ is the unit vector with spherical coordinate angles θ and ϕ, and λ is the wavelength corresponding to the angular frequency ω.

The previous formulation is generally considered when all the elements have an isotropic pattern. To consider non-isotropic element patterns, the classic theory provides the pattern multiplication principle, where the total frequency-wavenumber function is expressed as,

$$\Upsilon(\omega, \mathbf{k}) = \text{AF}(\mathbf{k})\Upsilon_e(\omega, \mathbf{k}), \qquad (5)$$

where $\text{AF}(\mathbf{k})$ is the array factor and $\Upsilon_e(\omega, \mathbf{k})$ is the frequency-wavenumber function of the single element.

Defined the general mathematical framework, it is clear from (1) and (5) that, for a given frequency, several aspects are determining the performance of the array [35]:

- the geometry of the overall array (linear, circular, rectangular, spherical, etc.), which impacts the manifold vector in (3);
- the complex weights of the individual elements, expressed in (2);
- the pattern of the individual elements, identified in (5).

In this paper, several geometries are evaluated, while the phase components of the complex weight vector are controlled to steer the main beam in the desired direction.

To complete the mathematical framework, it is useful to introduce the beam pattern function. The beam pattern is the frequency-wavenumber response function in (1) evaluated versus the direction,

$$B(\omega : \theta, \phi) = \Upsilon(\omega, \mathbf{k})|_{\mathbf{k} = \frac{2\pi}{\lambda} \mathbf{a}(\theta, \phi)}. \qquad (6)$$

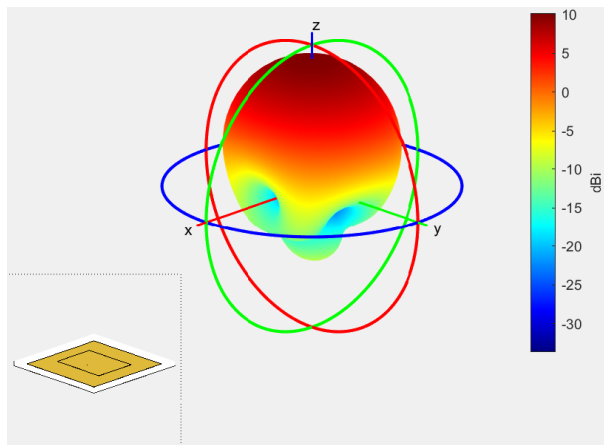The beam pattern is a key element to determine the performance of the array.

FIGURE 3. The 3D directivity beam pattern of the individual radiating element.

TABLE 1. Main parameters of the generic scenario.

Description	Parameter	Value
Element half power beam width	$HPBW^e$	$57°$
Element gain	G^e	$10\,\text{dBi}$
Swarm number of elements	N	-
Swarm distance between elements	d	-
Swarm total power	P_{tx}^s	$36.0\,\text{dBm}$
Swarm total gain	G^s	-
Center frequency	f_c	L/S-band
Wavelength at center frequency	λ	-
Swarm beam steering angles	(θ_s, ϕ_s)	-
Swarm half power beam width	$HPBW$	-
LEO altitude	h	$500\,\text{km}$
Elevation angle	ϵ	-
Beam footprint radius	r	-
UE antenna gain	G^{UE}	$0\,\text{dBi}$

b: DOWNLINK SYSTEM MODEL

The downlink model between the swarm equipped with N satellite, each with one radiating element, and a single user on the ground represents a single-user multiple-input single-output (SU-MISO) communication system. The received signal of the UE can be written as

$$y = \mathbf{h}^H \mathbf{w} x + z, \qquad (7)$$

where $\mathbf{h} \in \mathbb{C}^N$ is the far-field complex baseband channel vector, $\mathbf{w} \in \mathbb{C}^N$ is the complex weight vector in (2), $x \in \mathbb{C}$ is the transmitted signal symbol and $z \in \mathbb{C}$ denotes the circularly symmetric AWGN having zero mean and σ^2 variance, i.e., $\mathcal{CN}(0, \sigma^2)$. The vector $\mathbf{h}$ takes into account the geometry of the array represented by the manifold vector in (3) along with the path loss.

c: MAIN PARAMETERS

From a practical point of view, the swarm is composed of small satellites, e.g., 1U CubeSat. A 1U CubeSat platform can integrate all components, including solar panels, within a cubic shape of approximately $10 \times 10 \times 10$ cm size. The approximate weight is 1 kg, and 0.7 W is the available power). Each CubeSat is equipped with a single antenna that can be installed on its bottom deck. The antenna element is assumed to be a microstrip patch antenna optimized for the S-band with maximum directivity of 10 dBi and $57°$ of half power beam width. The antenna pattern used in the simulation is based on a commercial off-the-shelf product available in the catalog of a well-known manufacturer of small satellites [36]. Fig. 3 shows the 3D directivity beam pattern of the individual radiating element.

Regarding the orbit, a low Earth orbit with $h = 500\,\text{km}$ altitude represents an intermediate choice and a compromise between orbit parameters and propagation effects. Regarding the channel, the free space loss is the only considered impairment,

$$L_{fs} = (4\pi R_n/\lambda)^2, \qquad (8)$$

where R_n is the distance from the n-th swarm antenna to the UE. In particular, since the antenna aperture is generally small compared to the distance between each swarm element antenna and the UE, then $R_n \approx R$, where R is the distance between the center of the swarm and the UE.

On the terrestrial side, the reference UE is a terminal supporting L and/or S-band and 0 dBi antenna gain. Table 1 summarizes the main parameters of the defined generic scenario. Values not provided in this table are specified later during the evaluation.

2) KEY PERFORMANCE INDICATORS (KPIs)

The main KPIs utilized to define and compare the performance of the swarm are the following:

- **Maximum directivity** (D_{max}): the maximum directivity value of the main lobe; the directivity is the ratio of the radiation intensity in a given direction from the antenna to the radiation intensity averaged over all directions [35]; in the considered scenario, where the antenna losses are assumed negligible, the maximum antenna gain is equal to the maximum directivity; in the classical array theory [34] the directivity is expressed as,

$$D(\theta, \phi) = \frac{P(\theta_s, \phi_s)}{\frac{1}{4\pi} \int_0^\pi d\theta \int_0^{2\pi} d\phi \, \sin\theta \cdot P(\theta, \phi)}, \qquad (9)$$

where $P(\theta, \phi) = |B(\omega : \theta, \phi)|^2$ is the power pattern and B is the beam pattern function in (6).

- **Maximum minor lobe level** (MLL_{max}): the difference between the highest minor lobe's value and the main lobe's value, expressed in dB and usually negative; when the value is near 0 dB the pattern is affected by the grating lobes problem;

- **Half power beam width** ($HPBW$): the angular width (°), measured on the main lobe of an antenna radiation pattern at half-power points, i.e., the points at which the signal power is half (or -3 dB) of its peak value.

3) REQUIREMENTS AND DESIGN GOALS

From now on, the center frequency f_c is assumed to be 2 GHz (in S-band), so $\lambda \approx 0.15$ m. Regarding the requirements,

TABLE 2. Downlink channel - Link budget components.

Description	Parameter	Value	UM
Swarm total power	P_{tx}^s	36.0	dBm
Free space loss	L_{fs}	−152.4	dB
UE antenna gain	G^{UE}	0.0	dBi
UE receiver sensitivity power level	$P_{rx}^{UE}(ref)$	−89.6	dBm

as already mentioned, the UE is a common terrestrial device, like a 5G smartphone. The 3GPP/ETSI standard in [37] specifies the reference power levels that the UE has to receive to have the defined target performance. According to the standard, the reference values for a 5G UE at 2 GHz (specifically for the frequency band N1) and a QPSK modulation range from −100 dBm to −89.6 dBm, respectively for 5 MHz to 50 MHz of bandwidth. For this reason, considering the strictest value, the first requirement for the swarm's design considers P_{rx}^{UE} equal to −89.6 dBm as the reference received power level for the UE.

Considering the free space loss in (8) with $R = h$ (for a main beam in the nadir direction), a wavelength $\lambda \approx 0.15$ m, and a simple link budget formulation for the downlink channel, it is possible to translate the first requirement into the first design goal. The obtained first design goal is shown by the following inequality:

$$G^s \geq P_{rx}^{UE}(ref) - P_{tx}^s + L_{fs} - G^{UE} = 26.8 \text{ dBi}, \quad (10)$$

where the values are defined in Table 2.

The second requirement is related to the coverage of the main lobe shaped by the swarm. The target coverage is assumed to be a circular area with a radius from 3 to 5 km, which are common values for a terrestrial base station operating in 5G FR1 (Frequency Range 1 or Sub-6 GHz). With simple geometrical calculation and neglecting the Earth's curvature on this small area, it is possible to derive the *HPBW* angle in the function of the radius using $HPBW = 2\tan^{-1}(h/r)$ where h and r are graphically represented in Fig. 2. Thanks to this simple mathematical formulation, using the value of h in Table 1 and the extreme values of the considered radius $3 \leq r \leq 5$ km, it is possible to derive the second design goal:

$$0.68° \leq HPBW \leq 1.15°. \quad (11)$$

B. REFERENCE ARCHITECTURE

Considering the information in Section III-A, the design starts with a swarm based on a rectangular geometry, because it has a solid theoretical formulation coming from the phased array antenna theory. Recalling that each radiating element uses complex weights with identical magnitude and progressive phase, this array is known in the phased array theory as a uniform rectangular array or URA. In particular, the reference architecture considers a square geometry with elements displaced on a 2D plane of $\sqrt{N} \times \sqrt{N}$ positions and uniform inter-element distance d, as shown in Fig. 4.
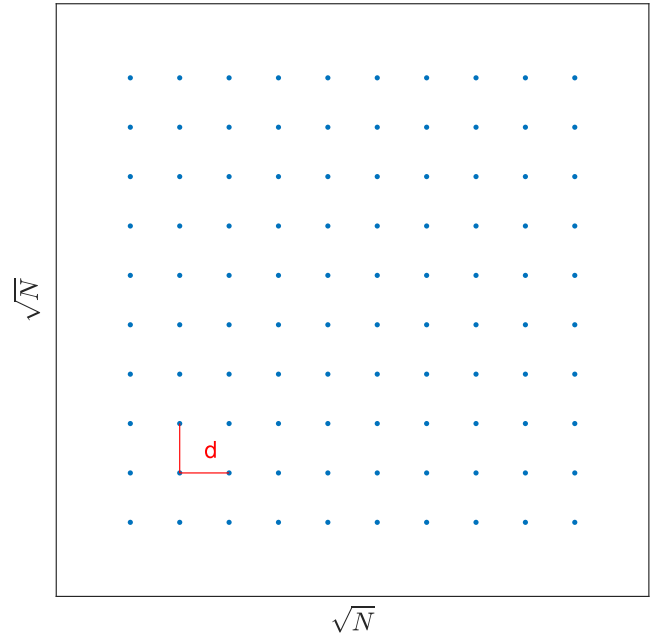

FIGURE 4. Uniform rectangular array (URA) with $\sqrt{N} \times \sqrt{N}$ elements and inter-element distance d.

There is an important consideration regarding the value of d for the rectangular geometry. When the distance d between the elements is equal to or greater than $\lambda/2$, the beam pattern presents several maxima of equal magnitude. The maximum in the desired direction is referred to as the major or main lobe, while the remaining unwanted lobes are called the grating lobes. Therefore, to have the possibility of steering the main beam in the entire visible region of the beam pattern, i.e., $\phi_s \in [0°, 360°)$ and $\theta_s \in [−90°, 90°]$ (Fig. 2), while avoiding the presence of grating lobes, it is necessary to respect the threshold imposed by $d \leq \lambda/2$ [35]. To be more precise, d can be higher than the previous threshold and up to λ when the required beam steering capability is limited. In contrast, a value of d greater than λ produces grating lobes in the visible region of the beam pattern. In satellite communication, the required beam steering capability can be geometrically derived according to the satellite orbit parameters. As an example, a geostationary orbit (GEO) satellite only requires a beam steering range of a few degrees to steer the main beam in its whole field of view. Hence, a higher value of d and a large reduction of the beam steering capability are generally accepted. On the other hand, a LEO satellite requires a large range of steering angles to steer the main beam in its whole field of view. In this case, a large reduction of the steering capability would also reduce the service area of the satellite and thus increase the number of swarms to achieve global coverage.

Recalling the design goals in (10), (11) and considering the main lobe in the nadir direction ($\theta_s = \phi_s = 0°$), the design of the array parameters follows these two approaches:

- set a static distance d and consider a variable number of elements N;
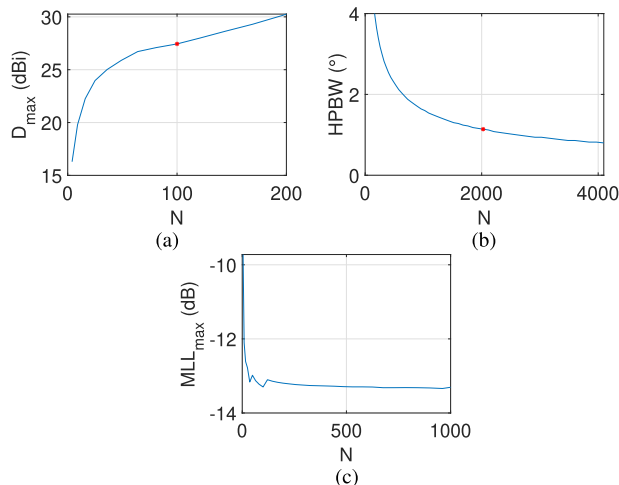
FIGURE 5. KPIs analysis of the URA with $d = \lambda$ and increasing N: (a) maximum directivity, (b) half power beam width, (c) maximum minor lobe level.

FIGURE 6. Unfolded BlueWalker 3 [7].

TABLE 3. Details of the architecture of BlueWalker 3 (derived from a visual reverse engineering process and several hypotheses).

Description	Parameter	Value	UM
Rows	R	14	-
Columns	C	12	-
Total positions	$T = R \cdot C$	168	-
Empty peripheral positions	$E1$	16	-
Empty central positions	$E2$	4	-
Number of tiles	$X = R - E1 - E2$	148	-
Elements per tile	Y	16	-
Number of elements	$N = X \cdot Y$	2368	-
Total aperture area	A_{total}	64.38	m^2
Tile area	$A_{tile} = \frac{A_{total}}{T}$	0.38	m^2
Tile side	$S_{tile} = \sqrt{A_{tile}}$	0.62	m
Tile row positions	R_{tile}	4	-
Element distance	$d = \frac{S_{tile}}{R_{tile}}$	0.155	m

TABLE 4. BlueWalker 3 simulated KPIs.

Sat	N	A_e (m^2)	D_{max} (dBi)	MLL_{max} (dB)	$HPBW$ (°)
BW3	2368	64.38	52.30	-13.9	1.12

- set a static number of elements N and consider a variable distance d.

1) CONSTANT D VARIABLE N

In the first approach, neglecting the beam steering capability, the distance d is set to $\lambda \approx 0.15$ m while the value of N is increased. Fig. 5 shows the results of the simulations. In particular, Fig. 5a shows that it is possible to fulfill the first design goal in (10) when $N \geq 100$. In this case, the array would be a square of about 1.5 m × 1.5 m, but with an HPBW of 5°, which means a beam footprint radius of about 22 km.

In contrast, Fig. 5b shows that the second design goal in (11) can be fulfilled only when $N \geq 2025$. As expected, MLL_{max} reaches a threshold that corresponds to the minimum level guaranteed by an ideal uniform array (Fig. 5c).

Although it is technically possible to realize an array with 2025 elements, the size of the array grows considerably. Considering $d = \lambda \approx 0.15$ cm, the size of a similar array would be a square of 7 m × 7 m. A structure of a similar dimension would be very difficult to carry in space unless using a deployable structure. This is exactly what AST Space-Mobile has been doing with its new unique concept. Before proceeding with the design of the swarm, given the similarity of BlueWalker 3 with the reference architecture, it is interesting to analyze its structure and draw some considerations.

a: BlueWalker 3 ARCHITECTURE

The BlueWalker 3 is a test satellite, developed by AST Space-Mobile, to test direct-to-cell connectivity using terrestrial mobile bands thanks to several mobile operator agreements. It is a massive satellite with a surface of about 64m^2 [7]. It is composed of multiple tiles connected by tapespring connectors. Each tile acts as a solar cell on one side and has an antenna array on the other side. It can be launched in a folded state on Earth and it can unfold in space without power consumption thanks to the lock forces generated by the
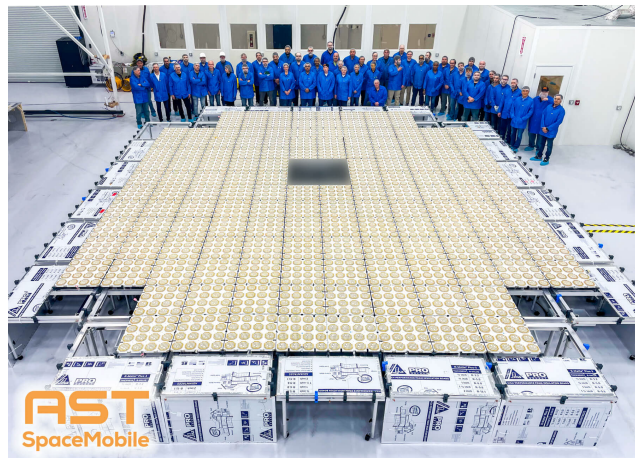
tapespring connectors [38]. Only a few technical details from the FCC application in [39] are available at the moment, but it is possible to derive some rough technical details through a visual reverse engineering process of Fig. 6. In particular, by making some hypotheses, the data in Table 3 can be derived. Considering the derived details and a center frequency f_c=2 GHz, it is possible to simulate the BlueWalker 3 architecture and evaluate its KPIs. For this purpose, the manifold vector in (3) is modified considering the element positions in Fig. 7. Considering a complex weighting vector with uniform amplitude and progressive phase a representative 2D cut of the directivity is shown in Fig. 8. The resulting KPIs performance is summarized in Table 4. It must be emphasized that the values derived in Table 4 are only based on a simulation under several simple assumptions. In addition, the simulation considers that all the N radiating elements of the array are used for the transmission at the same time and
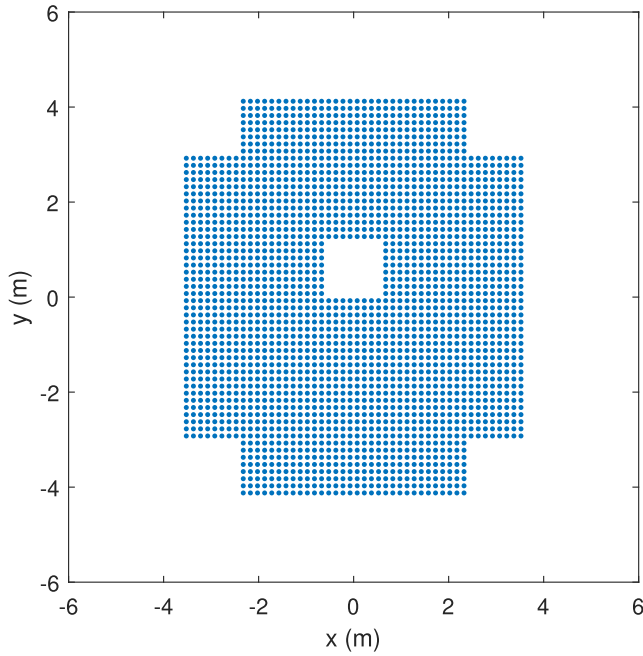
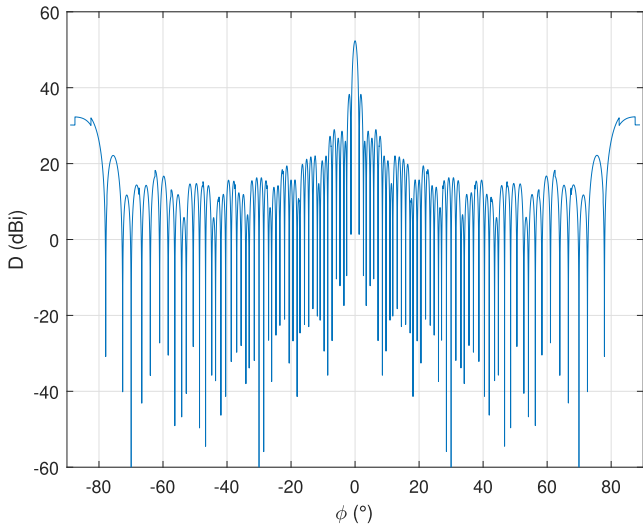**FIGURE 7.** BlueWalker 3 derived geometry.

FIGURE 8. BlueWalker 3 simulated 2D directivity cut.

uniform amplitude of the complex weights. According to the FCC application in [39], it uses only a subset of the available tiles and a Chebyshev taper function to reduce the secondary lobe level (SLL). In particular, it uses a limited subset of tiles when the satellite is beamforming at the broadside and a larger number of tiles when the main beam is steered in different directions. The provided directivity values range from 39 to 46 dBi for a steering angle ranging approximately from 0 to 60° [39]. Furthermore, the LEO altitude is 730 km and the target beam radius is 12 km.

Concluding this parenthesis on the BlueWalker 3, although its deployable structure solves the problem to fit the satellite into the rocket, it also increases the complexity of building
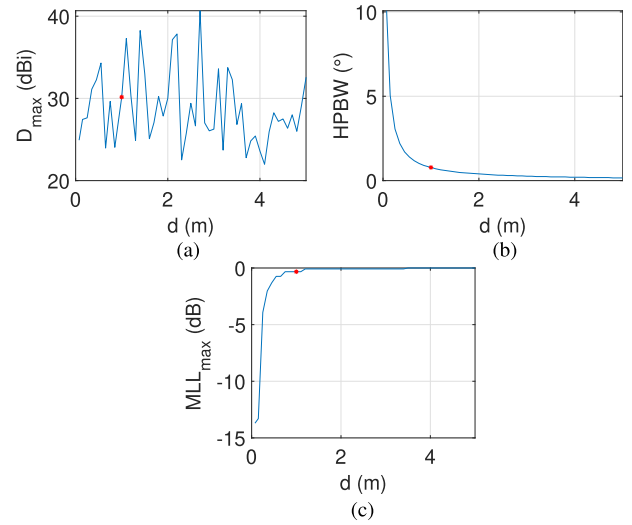

FIGURE 9. KPIs analysis of the URA with $N = 100$ and increasing d: (a) maximum directivity, (b) half power beam width, (c) maximum minor lobe level.

the satellite and it does not reduce the weight, consequently, it does not reduce the build/launch cost.

2) CONSTANT N VARIABLE D

Continuing the swarm design, in the second step, based on the results from Fig. 5, the number of elements is now fixed to $N = 100$ while the inter-element distance d is varied. Fig. 9 shows the results of the simulations. In particular, Fig. 9b shows that when $d = 1$m (i.e., 6.67λ at $f_c = 2$ GHz) the *HPBW* value is in the range provided by (11). Unfortunately, as expected and shown in Fig. 9c, the increase of the element spacing leads to the grating lobe problem. Furthermore, the grating lobe problem leads to the erratic behavior of Fig. 9a. It can be demonstrated that the directivity behavior of an array matches exactly the directivity behavior of a continuous aperture with the same area only when the continuous aperture is sampled with elements equally spaced up to $\lambda/2$. Sampling a continuous aperture with elements with larger spacing leads to the grating lobe problem that is identical to the problem of aliasing in time series analysis, which occurs when the time domain waveform is under-sampled [34]. New grating lobes come into the visible space of the beam pattern every multiple of λ generating sharp dips [40] as in Fig. 9a.

To summarize, the results from Fig. 5 and 9 lead to the following conclusions:

- in the first step of Fig. 5, keeping the inter-element distance constant at $d = \lambda$ and increasing the number of antenna elements would require $N \geq 2025$ to fulfill the design goals in (10) and (11);
- in the second step of Fig. 9, fixing the number of antenna elements to $N = 100$ and increasing the inter-element distance is, on the other hand, sufficient to satisfy both (10) and (11) but, in this latter case, grating lobes impair the beam pattern.
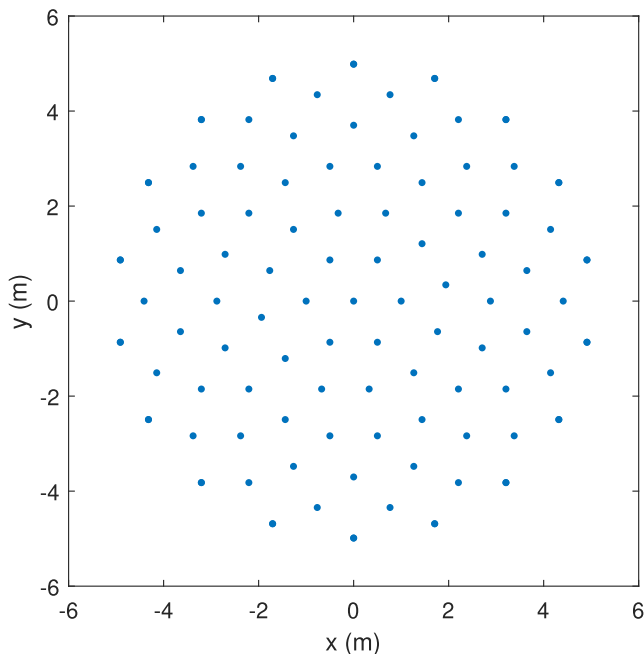
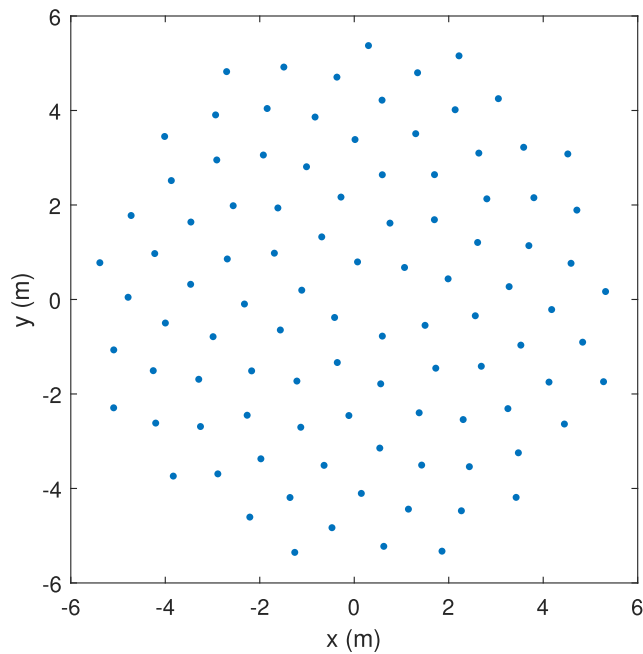**FIGURE 10.** ASA geometry with $N = 109$ and $d = 1$m.

FIGURE 11. LSA geometry with $N = 100$ and $d = 1$m.

The mitigation of the grating lobes is hence a key aspect to design swarms with a reasonable number of elements. This will greatly reduce the costs especially due to the limitation of the total launch weight of the system.

C. IMPROVED ARCHITECTURES

In the scientific literature, there are several strategies for approaching the grating lobe problem. An interesting approach relies on the displacement of the elements as in [13], [14], [15], [16], and [17]. The common idea is to interrupt the periodic element distance present in the conventional geometries that permit the in-phase addition of radiated fields in more than one direction generating the grating lobes.

The analysis conducted in this paper considers only 2D geometries to understand the basic design trade-offs and evaluate the potential of the swarm approach. However, introducing an additional radius of curvature along the third dimension of the swarm geometry could, for example, improve the directivity and HPBW of the scanned lobes [41], [42], [43]. Nevertheless, further studies are needed to identify a clear advantage of 3D geometries in large sparse and high inter-element distance arrays such as in the swarm scenario.

In this paper, the following geometries are considered:

- the augmented spiral array (ASA) from the patent in [44];
- the logarithmic spiral array (LSA) from the patent in [45];
- the enhanced logarithmic spiral array (ELSA), defined in this document.

Although the first two geometries have been already considered in previous works, their performance at high inter-element distances has never been tested before.

1) AUGMENTED SPIRAL ARRAY (ASA)

The first considered geometry is the augmented spiral array (ASA) from the patent [44]. It is based on a spiral geometry and it is composed of different structures: a six-fold core lattice configuration in the center with 19 elements and multiple 18-fold annular rings. Due to the formulation, it is not possible to create an array with an arbitrary number of elements. Fig. 10 shows the ASA configuration with $N = 109$ (the nearest possible value to $N = 100$) and $d = 1$m.

2) LOGARITHMIC SPIRAL ARRAY (LSA)

The second considered geometry is the logarithmic spiral array (LSA) from the patent [45]. It has a very simple formulation described by the following equation expressed in polar coordinates

$$\rho_n = \frac{d}{\sqrt{\pi}}\sqrt{n} \text{ and } \phi_n = 2\pi\tau n, \quad n = 1, \dots, N, \quad (12)$$

where every point is defined by the couple (ρ, ϕ). The value of ρ represents the distance from the central reference point and ϕ the angle from the reference direction. It depends on the element number n (ranging from 1 to N), the equivalent one-dimensional linear spacing between one antenna element to another d and the golden ratio

$$\tau = \frac{1 + \sqrt{5}}{2} \approx 1.618. \quad (13)$$

The LSA maintains a substantially uniform cell size per element. However, it does not have the periodic linear spacing of the rectangular geometry. Thanks to its formulation, every value of N can be selected. Fig. 11 shows the LSA configuration with $N = 100$ and $d = 1$ m.
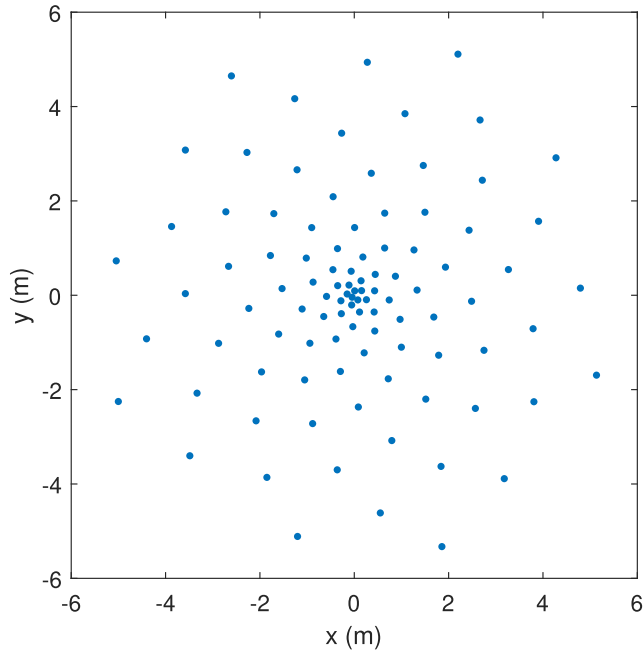
FIGURE 12. ELSA geometry with $N = 100$, $d = 1$ m and $st_c = 0.1$.

FIGURE 13. KPIs analysis of the ELSA with $N = 100$, $d = 1$ m and st_c from 0 to 1: (a) maximum directivity, (b) half power beam width, (c) maximum minor lobe level.

3) ENHANCED LOGARITHMIC SPIRAL ARRAY (ELSA)

An interesting solution built upon the LSA geometry is the spatial tapering from [13]. In this work, the authors emulate a Taylor amplitude taper by varying the radiator distance from the center to obtain a reduction of SLL. In other words, it is possible to obtain better performance in terms of SLL when the elements in the center of the array are closer than the elements in the periphery of the array. A similar concept is also applied to the SpaceX patent [46]. Although the impact of this strategy is mainly on the SLL and not on all the minor lobes, it is worth trying and examining the results. Thanks to these observations, a generalized version of the LSA is derived in this document.

The enhanced logarithmic spiral array (ELSA) has the same mathematical formulation as the LSA with a modification in the definition of d. In particular, it introduces the parameter d_n that is a function of the element number n, the value of d and the coefficient st_c that controls the level of the spatial tapering. The following formulation

$$\rho_n = \frac{d_n}{\sqrt{\pi}}\sqrt{n} \text{ and } \phi_n = 2\pi\tau n, \quad n = 1, \ldots, N \quad (14)$$

describes the radius and the angle of the n-th element, while the parameter d_n is described by

$$d_n = \left(\frac{d(1 - st_c)}{N}\right)n + (d \cdot st_c) \quad n = 1, \ldots, N. \quad (15)$$

The st_c parameter is in the range defined by

$$0 \leq st_c \leq 1, \quad (16)$$

and it defines the level of spatial tapering. When $st_c = 1$ the ELSA geometry becomes the LSA geometry. Fig. 12 shows the ELSA geometry for $st_c = 0.1$.
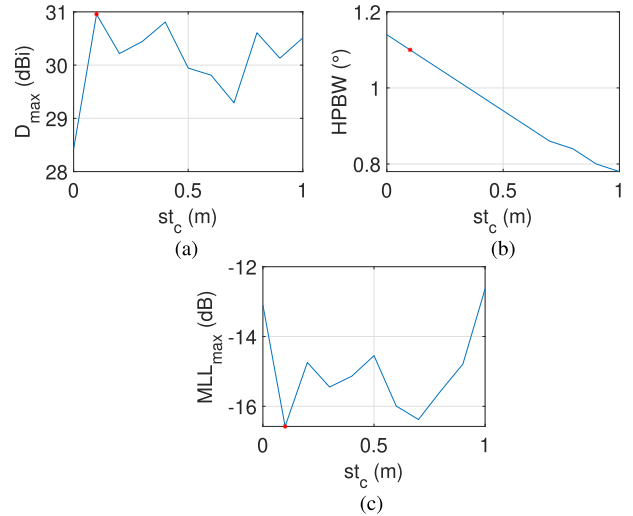
D. KPIs COMPARISON

1) BROADSIDE ANALYSIS

The following analysis considers the performance evaluation when the maximum radiation of the array is directed normally to the axis of the array, which is usually referred to as the broadside direction. Referring to Fig. 2, the steering angle is $\theta_s = \phi_s = 0°$.

Before comparing the reference and improved geometries, it is necessary to derive the best spatial tapering coefficient st_c for the enhanced logarithmic spiral array. Fig. 13 shows the behavior of the three KPIs in the function of st_c. The ELSA achieves its best results in terms of directivity (Fig. 13a) and minor lobe level (Fig. 13c) when $st_c = 0.1$. It is necessary to note that the value $st_c = 0.1$ is the best choice only for the current specific configuration. Different values of N, d, f_c lead to different results, hence a different value of st_c. In addition, in this simple optimization process, only one 2D cut of the total beam pattern is considered, but the geometry is not symmetrical to the coordinate reference system. As a result, different 2D cuts may perform slightly differently.

It is also necessary to note that the variation of the spatial taper only emulates the amplitude variation of the complex weights of the elements. As it is known from classical theory, an appropriate tapering of the excitation amplitude between elements can be used to control the HPBW and SLL. The smoother the taper from the center of the array toward the edges, the lower the SLL and the higher the HPBW, and vice versa. Therefore, a very smooth taper would result in a very low SLL but higher HPBW. In contrast, an abrupt distribution, such as that of uniform illumination, exhibits the smallest HPBW but the highest SLL [35]. The decrease of the spatial tapering coefficient, from 1 (LSA) to lower values, only emulates this effect by alternating smooth and abrupt transitions between the elements. This emulation produces
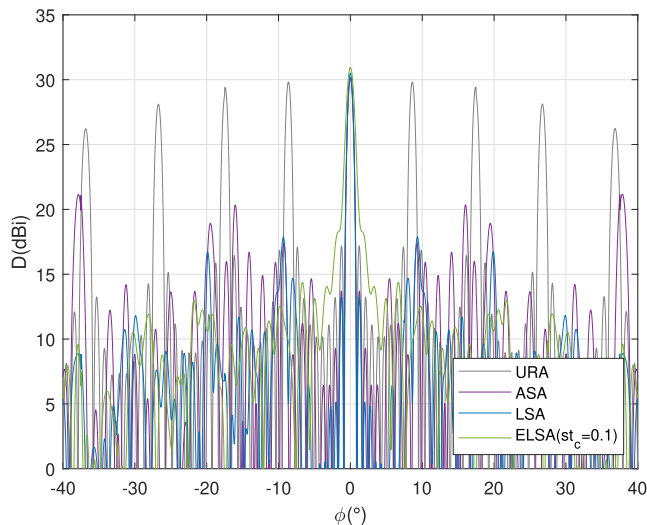
FIGURE 14. ASA, LSA and ELSA ($st_c = 1$) directivity 2D cuts comparison.

TABLE 5. Broadside KPIs comparison of URA, ASA, LSA and ELSA with similar configurations.

Geometry	N	A_e (m²)	D_{max} (dBi)	MLL_{max} (dB)	$HPBW$ (°)
URA	100	100.00	30.20	-0.33	0.78
ASA	109	97.02	30.12	-8.99	0.80
LSA	100	114.49	30.51	-12.63	0.78
ELSA	100	106.08	30.96	-16.58	1.10

the erratic behavior of the D_{max} and the MLL_{max} as shown in Fig. 13a and 13c.

Selected $st_c = 0.1$ it is possible to compare the different geometries. The simulation results of the URA, ASA, LSA and ELSA are compared in Fig. 14 with a superposition of their 2D directivity cuts. For a better comparison, the KPI's results for all the geometries are also summarized in Table 5, where A_e, not previously defined, is the equivalent aperture area generated by the geometry.

Finally, it is possible to observe, from the values in Table 5 and the graphs in Fig. 14, that all the improved geometries can mitigate the grating lobes with different performance. There is not a large difference compared to D_{max}, but there is a trade-off between LSA and ELSA. LSA performs better in terms of $HPBW$, while ELSA performs better in terms of MLL_{max}. Both outperform the ASA.

Although better performance (SLL around $-20\,\text{dB}$) can be achieved by considering random antenna arrays [47], the organized irregularity present in the spiral geometry brings advantages in the practical aspects of swarm implementation (Section V-A2.a).

2) BEAM STEERING ANALYSIS

It is interesting to characterize the geometries in terms of beam steering performance because the maximum steering angle defines the maximum coverage of the satellite. The principle of steering arrays is primarily based on control of
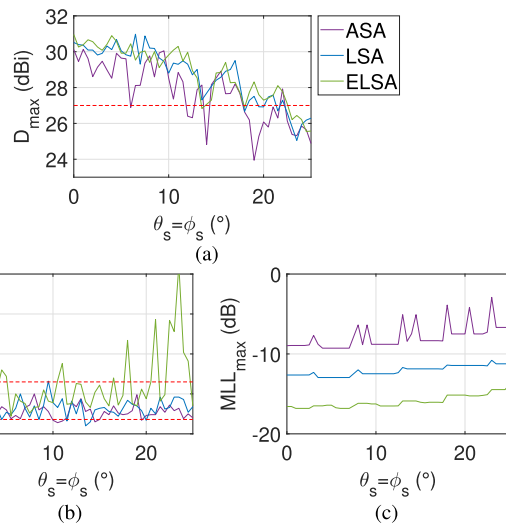

FIGURE 15. KPIs of the LSA with $d = 1$, $N = 100$ and $\theta_s = \phi_s$ from 0° to 25°: (a) maximum directivity, (b) half power beam width, (c) maximum minor lobe level.
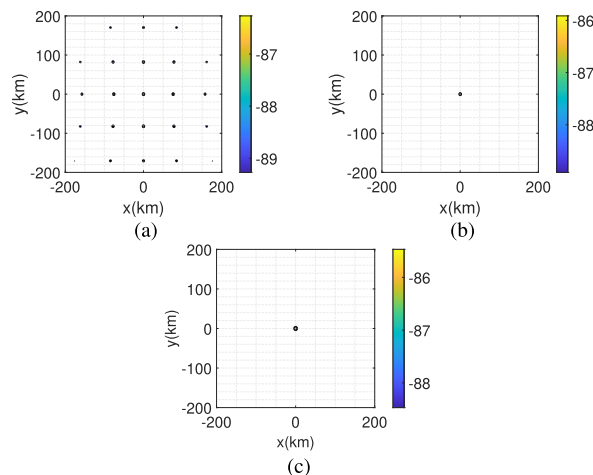

FIGURE 16. Beam pattern projection on a 400 × 400 km Earth surface: (a) URA with grating lobe problem, (b) LSA, (c) ELSA ($st_c = 0.1$).

the phase excitation of the elements. Controlling the phase, the maximum of the array pattern can be pointed in different directions.

This analysis considers $\theta_s = \phi_s$ ranging from 0 to 25°. Fig. 15 shows a comparison of the beam steering simulation results. The results confirm the broadside analysis. ELSA and LSA have similar performance and outperform ASA in terms of D_{max} (Fig. 15a). Furthermore, ELSA and LSA satisfy the first design goal described by the inequality in (10) up to around $\theta_s = \phi_s = 20°$. Observing Fig. 15c, ELSA achieves better performance in terms of MLL_{max}, but LSA and ASA show better results in terms of $HPBW$ (Fig. 15b). In particular, LSA and ASA fulfill the second design goal (11) for all the considered steering angles, while ELSA presents some values outside the design goal.
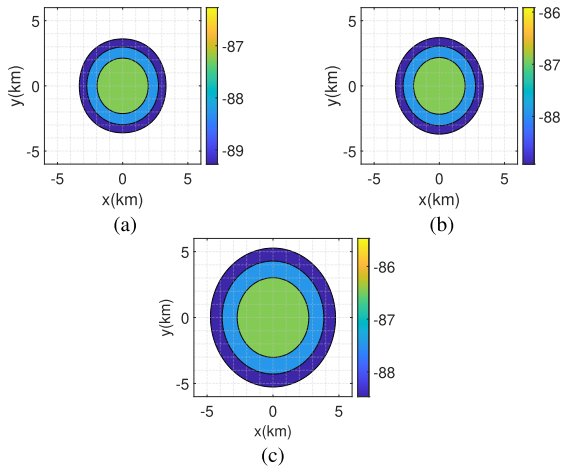
FIGURE 17. Beam pattern projection on a 12 × 12 km Earth surface: (a) URA main beam, (b) LSA main beam, 9c) ELSA ($st_c = 0.1$) main beam.

FIGURE 18. Beam pattern projection on a 450 × 450 km Earth surface: (a) LSA, (b) ELSA ($st_c = 0.1$).

FIGURE 19. Beam pattern projection on a 16 × 16 km Earth surface: (a) LSA, (b) ELSA ($st_c = 0.1$).

E. COVERAGE COMPARISON

1) BROADSIDE ANALYSIS

Simulating the projection of the beam pattern onto the Earth is an easy way to show the coverage of the main lobe and the effect of the grating lobes. The simulation considers the parameters previously described in Table 1, $\theta_s = \phi_s = 0°$, the Earth's curvature and a minimum pixel resolution of $250 × 250$ m. Again, the free space path loss is the only considered channel impairment. The values on the projections show the received power in dBm contained in the range $[P_{rx}^{UE}(max) - 3dB, P_{rx}^{UE}(max)]$, where $P_{rx}^{UE}(max)$ is the maximum received power on Earth. The color bar on the right side of each figure shows the received power's level in dBm.

Fig. 16 shows the projection on a $400 × 400$ km Earth surface. In particular, Fig. 16a is the projection of the URA beam pattern which clearly shows the grating lobes, while the projections of the other two beam patterns, respectively Fig. 16b for the LSA and Fig. 16c for the ELSA, do not show grating lobes.

Fig. 17 shows the projection on a smaller area, $12 × 12$ km, to highlight the projection of the main lobe. As the HPBW values in Table 5, Fig. 17a for the URA and 17b for the LSA show a similar coverage of the main lobe, while Fig. 17c for the ELSA shows an increased coverage of the main beam.

2) BEAM STEERING ANALYSIS

With the same considerations for the broadside case, the beam steering simulation considers the parameters described in Table 1, but with $\theta_s = \phi_s = 20°$. Fig. 18 shows the projection results for the LSA and ELSA($st_c = 0.1$) geometries. The effects of the steering are visible in Fig. 18a and 18b where the main beam is in the upper right side of the plot and not in the center as in the broadside simulation. Due to the additional distance to reach the surface along with the drop generated from the Earth's curvature, in this case, the main lobe's shape is more elliptical than circular as is shown in 19a and 19b.
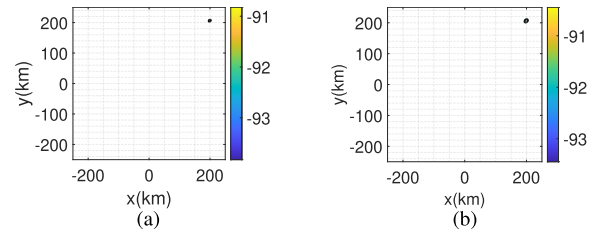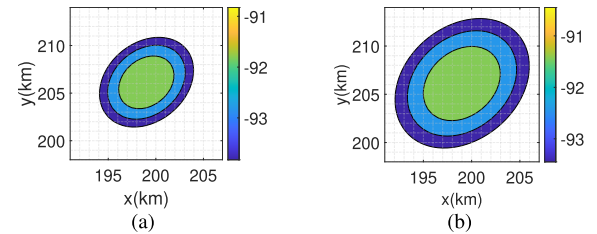
Furthermore, there are two important considerations:

- considering the received power level in the color bar, on the right-hand part of Fig. 18 and 19, it is lower than the first requirement for the swarm's design, P_{rx}^{UE} equal or greater than -89.6 dBm;
- considering the coverage of the beam in Fig. 19b, it exceeds the second requirement for the swarm's design (r from 3 to 5 km).

IV. FUTURE RESEARCH DIRECTIONS

Although the geometric design of the array is a crucial aspect, it is only one of the challenges related to the swarm system. Therefore, this section summarizes the main research directions that need to be further investigated.

A. BEAMFORMING OPTIMIZATION

Section III analyzed the swarm geometry to understand the swarm design trade-offs in terms of the identified KPIs. The obtained results are encouraging, but further efforts should be invested in:

- the minimization of the interference level outside the desired direction;
- the optimization of the beam steering capabilities.

In classical array theory, where the spacing between the elements is chosen to avoid grating lobes in the beam pattern, the secondary lobe level (SLL) can be avoided via taper functions (e.g., Hamming window). In this latter case, the amplitudes of the beamforming coefficients are weighted following a predetermined pattern. This approach works with regular geometries and common spacing between the elements, but the applicability to the LSA/ELSA geometry with high element spacing has to be analyzed. For this purpose, interesting similarities with the concentric circular antenna arrays (CCAA) can be exploited to benefit from previous works, for example [48], [49].

The results in Section III-D2 shows a maximum scan angle of 25° to meet the first design goal (10), i.e., the required minimum directivity. Furthermore, the results in Section III-E2 shows a degradation of the performance at the edges of the beam, which may lead to not meeting the design goals. For those reasons, when a specific scan area needs to be considered, it is necessary to carefully derive the design goals based on the extreme values of the scan area and to consider the performance at the edges of the beam.

Single beam analysis is important for understanding the trade-off of the swarm-based antenna array, but its full potential can only be achieved by considering the generation of multiple beams and the provision of services to multiple users. For this reason, the multi-user scenario plays a central role in the beamforming optimization of swarms.

1) MULTI-USER SCENARIO OPTIMIZATION

In the multi-user scenario, the swarm, a distributed phased array with a massive number of antenna elements, has to serve several users. For this purpose, the swarm must be able to create a flexible multiple beam coverage to enable efficient reuse of the available frequency resources and, hence, support a large number of users.

In this scenario, the downlink model in (7) must be extended. The swarm is equipped with N satellites, each with one radiating element, and K single antenna users, each served by one beam, are distributed on the ground. The received signal vector $\mathbf{y} \in \mathbb{C}^K$ can be written as

$$\mathbf{y} = \mathbf{H}^H \mathbf{W} \mathbf{x} + \mathbf{z}, \qquad (17)$$

where $\mathbf{H} \in \mathbb{C}^{N \times K}$ is the far-field complex baseband channel matrix, $\mathbf{W} \in \mathbb{C}^{N \times K}$ is the complex weights matrix, $\mathbf{x} \in \mathbb{C}^K$ is the transmitted signal symbol vector and $\mathbf{z} \in \mathbb{C}^K$ denotes the vector with K samples of circularly symmetric AWGN having zero mean and σ^2 variance, i.e., $\mathcal{CN}(0, \sigma^2)$. The channel matrix $\mathbf{H}$ can be expressed as

$$\mathbf{H} = [\mathbf{h}_0 \, \mathbf{h}_1 \, \cdots \, \mathbf{h}_{K-1}], \qquad (18)$$

where the vector $\mathbf{h_k}$ is the channel response between the N swarm elements and the k-th UE, taking into account the geometry of the array represented by the manifold vector in (3) along with the path loss effects. The complex weights matrix $\mathbf{W}$ can be expressed as

$$\mathbf{W} = [\mathbf{w}_0 \, \mathbf{w}_1 \, \cdots \, \mathbf{w}_{K-1}], \qquad (19)$$

where the vector $\mathbf{w_k}$ is the complex weight vector between the N swarm elements and the k-th UE as the one introduced in (2).

It follows that the signal received by the k-th UE can be represented as,

$$y_k = \mathbf{h}_k^H \mathbf{w}_k x_k + \sum_{k' \in \mathcal{K} \setminus k} \mathbf{h}_k^H \mathbf{w}_{k'} x_{k'} + z_k, \qquad (20)$$

where the first term is the useful signal and the second term is the interference from the other beams. In this mathematical framework, the coefficients of the complex weights matrix ($\mathbf{W}$) have to be optimized according to a defined criterion.

There is an extensive research background that can be used in this context. Optimization can be performed by using standard techniques for generic interference channels [50], e.g., min-rate maximization, weighted sum-utility maximization, QoS-constrained power minimization or by heuristic approaches, e.g., maximizing the signal-to-leakage-plus-noise ratio (SLNR) [51]. It should be noted that optimization approaches based on signal-to-noise and interference ratio (SINR) are valid for creating multiple beams over the defined user locations, but they do not take into account the level of energy transmitted from the array to the entire coverage area. The optimization process must consider the amount of energy transmitted in the entire service area to ensure the absence of grating lobes. Considering the ELSA geometry proposed in Section III-C, the st_c value could be taken into account during the optimization process to define the best spatial tapering level of the geometry.

Furthermore, in recent years, massive multiple-input multiple-output (mMIMO) transmission has been developed for terrestrial cellular wireless networks [52], [53]. This technique provides solutions for the efficient formation of multiple beams in systems with a large number of antennas. Therefore, it is a promising strategy to be used in this context. The literature on the mMIMO technique in LEO satellite systems is limited, but interesting recent work [54], [55] opens up promising developments for swarm-based antenna arrays.

B. SYNCHRONIZATION METHODS

The swarm is a distributed satellite system (DSS) where several individual nodes transmit and receive signals coherently, creating a distributed phased array. Time and frequency/phase synchronization are essential to guarantee the expected beamforming performance. The synchronization task is challenging when the nodes are physically separated and in relative motion, which is the case of the swarm in free-flying formation. The navigation satellite systems provide synchronization capabilities that are not sufficient to support phase coherence at microwave frequency [56]. Hence, other approaches have to be investigated. According to the research literature, two main approaches are available to face this problem: the closed-loop and open-loop strategies [56], [57]. Although these schemes are different approaches, sometimes it is hard to make a clear distinction between open loop and closed loop because they use similar principles.

1) CLOSED-LOOP

The closed-loop method, as presented in Fig. 20a, uses a feedback loop from the beamforming destination to the distributed satellite system. There are two main implementations, the full-feedback and one-bit feedback [57].

In the full-feedback implementation, the destination broadcasts a beacon and all the nodes of the DSS "bounce" the signal back to the destination using a code domain

multiple access (CDMA) scheme. The destination estimates the phase differences of the received signals and sends phase compensation messages via CDMA to all nodes. Each node can use the message to update its state. If the phase offsets have not changed during the process, the desired degree of phase convergence is achieved with one iteration.

In the one-bit feedback implementation, the nodes of the DSS randomly adjust their states and transmit to the destination as a distributed beamformer. The destination performs a signal-to-noise ratio (SNR) measurement and broadcasts a bit of feedback. The state of the bit indicates whether the measured SNR is better or worse than the previous transmission. The nodes of the DSS can update their states according to this information. In this case, the complexity of the algorithm defines the needed number of iterations to achieve the desired degree of phase convergence.

Another interesting implementation is from the patent in [58]. In this implementation, the nodes of the DSS select an initial set of weights and transmit a signal to the destination as a distributed beamformer. The destination measures several metrics of the received signal (e.g., the received power) and it transmits back the results of the measurement. The DSS uses the received measurements, computes a newly optimized set of weights and transmits the signal again. The optimization of the new set of weights can be done in different ways, e.g., using the gradient of SNR of the received feedback.

Although the closed-loop method requires little or no coordination between the nodes of the DSS, it has several drawbacks. The beamforming destination is involved in the synchronization process and the set of weights is optimized only for the location of the beamforming destination. Furthermore, in satellite communication, where the distance between the endpoints is large, the feedback delay due to wave propagation must be carefully considered. A long feedback delay could lead to an outdated set of weights and thus beamforming in the wrong direction.

The use of the closed-loop method in direct-to-cell connectivity with swarms also presents other problems. Closing the link between each satellite of the swarm and the UE is not possible due to the low gain of the radiating elements and the large distance. It may also be difficult to close the link with the swarm and the UE when a random initial set of weights is selected. In addition, involving the UE in the synchronization process would add processing complexity and power consumption. In particular, for implementation based on the full feedback, where a beacon signal is needed to start the process, due to UE power limitation, the resulting beacon signal transmitted by the UE would be weak, noisy and hence unreliable.

2) OPEN-LOOP
On the other hand, the open-loop approach in Fig. 20b does not rely on a feedback loop with the beamforming destination. In this case, the nodes have to self-align through higher cooperation. The open-loop distributed beamforming is more complex and generates several potential errors that have to be
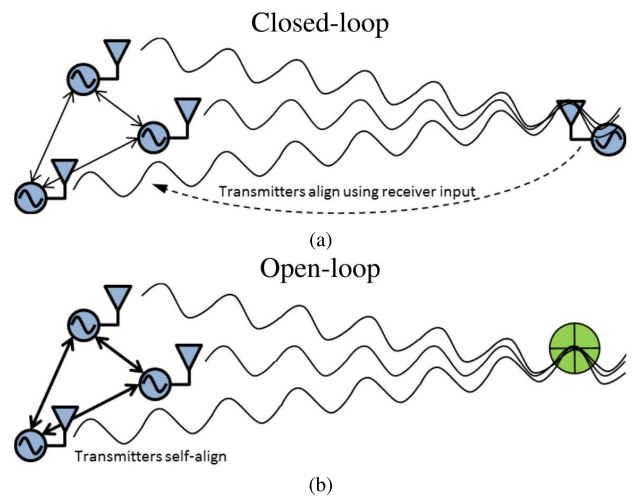

FIGURE 20. Distributed phased array synchronization methods (pictures from [59]): (a) closed-loop method, (b) open-loop method.

controlled and/or mitigated. In particular, three main errors are the most stressful: internode range, node orientation and phase alignment of the clocks on each node [59].

The internode range estimation can be done using RF or optical signals. Methods with RF signals are more technologically mature and easier to implement compared to the ones with optical signals. Optical signals can achieve better performance but they need pointing, acquisition and tracking capabilities that increase the performance requirements and hence the complexity of the nodes. In the swarm context, where each node is a small satellite with limited performance and a high number of satellites is considered, the creation of a network of optical inter-satellite links (ISLs) is a complex task. An alternative approach is to broadcast a strong beacon signal from a reference station while the distributed system adjusts its weights by following different approaches, similar to those illustrated in the closed-loop section. The reference station could be a ground station, a terrestrial base station or a satellite. The choice of a satellite is the most attractive alternative. As stated in the introduction and shown in Fig. 1, the swarm usually has one satellite with more processing capabilities called the leader satellite, which can also be used as a reference for the calibration process.

Regarding node orientation, recent research has been based on the use of GPS. For the swarm approach, systems based on differential GPS (DGPS) methods can represent an interesting solution thanks to the achieved level of accuracy [60].

In the case of phase alignment, one-way clock methods are used in wired systems because the channel remains static. In one-way clock methods, the leader node sends a reference signal to the follower node which generates a local clock signal using a phase-locked loop (PLL) system. In wireless systems, a two-way clock transfer method can mitigate the dynamic channel conditions, but it introduces additional overhead. However, when a system for the internode range

estimation is already implemented the one-way clock transfer system can also work in wireless channels [59].

C. IMPERFECTION ANALYSIS

In distributed beamforming, the signals emitted by the swarm elements have to arrive at the UE in phase and with sufficient relative timing such that the signals add constructively to increase the total signal power. In the case of reception, the relative phase and timing of the received signals have to be aligned to achieve coherent and cooperative processing. In Section III the swarm-based antenna array has been designed considering the perfect stability and synchronization between satellites. In practice, several imperfections can degrade the beamforming performance.

The work in [56] describes several factors impacting distributed coherence and accuracy. These factors must be estimated and corrected to ensure the required level of coordination. A non-exhaustive list of factors includes:

- relative oscillators: time-varying phase shift from imperfect oscillator synchronization and phase noise;
- distance between each node and a reference location;
- relative timing offsets;
- phase delays through each transceiver system;
- antenna phase pattern for each node;
- vibration on the platform;
- antenna depolarization;
- doppler errors from relative platform motion;
- geometric differences between antenna phase centers.

Considering the swarm approach, some of these factors can be mitigated or neglected. In particular, the single antenna of the swarm element is a wide-beam antenna with quite a constant phase pattern in the main beam. Different from UAVs, the platform vibrations are minimal on satellites. Antennas with circular polarization can minimize the impact of depolarization. Doppler shift effects between nodes can be neglected considering that the swarm is organized in a formation flying that is responsible to maintain a defined geometry. Finally, using the same antenna for the internode range estimation and the beamforming can mitigate the differences between the phase centers of the antennas.

Previous works in [27], [59], and [61] have already investigated the performance degradation of distributed systems through a statistical characterization of the phase error. Particularly interesting are the results presented in [27] in which the authors studied a swarm of CubeSats for deep-space communications in the X-band. The results obtained using the mathematical model derived in [62], show a beamforming degradation of the gain (array loss) or around -3dB for swarms with 100 elements.

In addition, since the grating lobes are mitigated by breaking the periodicity of regular geometries, a large degradation of the performance when the proposed geometry varies from the correct one is not expected. Most importantly, the relative positions between the satellites must be estimated with a certain degree of accuracy and the beamforming coefficients updated accordingly. The work [59] suggests an

estimation accuracy of cm-level to limit the degradation of the beamforming performance. This level of accuracy could be achieved with synchronization methods based on RF and differential GPS technologies [59], but a thorough characterization of the performance losses induced by the impairments previously listed is needed.

Understanding the range of possible errors that the swarm can tolerate is one of the most important challenges to orient the decisions for the system design. Therefore, further efforts should be invested in this area of research, especially for the feasibility of the free-flying swarm configuration.

1) MUTUAL COUPLING EFFECT

It is worth noting that the previous list does not include an important effect of antenna arrays, mutual coupling. It is generally agreed that mutual coupling cannot be omitted in dense arrays, i.e., when the average element spacing is less than about half a wavelength [63]. However, analyses in [40] and [64] show that the impact of the mutual coupling is reduced when the inter-element distance increases. In particular [64] presents the analysis of a planar array with patch antennas, and concludes that the effect can be neglected when the distance between elements is more than half the wavelength.

The ASA and LSA geometries discussed in the article have a distance between elements of about 6.67λ. As for ELSA with the minimum spatial tapering coefficient $st_c = 0.1$, the minimum distance between elements is of about λ (Section V-A1.a).

Therefore, it is reasonable not to expect large power losses due to impedance mismatch or an alteration of the total beam generated by the mutual coupling effect.

V. SYSTEM DESIGN ASPECTS

Despite the research directions identified in the previous section, it is necessary to recognize the importance of other aspects critical to the feasibility of the swarm-based approach. This section presents an overview of the most important system design aspects.

A. SWARM CONFIGURATIONS

Although hybrid solutions are possible, the swarm can be arranged in two configurations, the free-flying configuration (i.e., wireless connected) or the tethered configuration (i.e., wired connected). Fig. 1 shows a graphical representation of both configurations in an operative example scenario. They present different challenges/opportunities and advantages/disadvantages that need to be highlighted.

1) FREE-FLYING SWARMS

When a free-flying swarm is considered, formation flying (FF) stability is one of the main challenges. The FF has to be kept stable during the flight around the Earth. Several effects like Earth's oblateness, atmospheric drag and solar radiation pressure significantly affect the positions of the swarm elements, necessitating periodic orbit corrections to maintain stability. An approach to the FF's stability relies on the study of the orbit dynamics. An interesting publication

in this field is [65]. It presents a swarm-keeping strategy that means maintaining relative distances between multiple satellites in the presence of disturbances and ensuring that collisions do not occur. The study is of particular interest because it considers the formation of hundreds of small satellites in LEO orbit. The proposed method consists in applying a set of initial conditions to the satellites of the formation to provide collision-free trajectories. The numerical results show that the average drift of the satellite position in the formation is reduced from m/orbit to mm/orbit. Other interesting publications using free-flying swarms are in [25], [26], and [27].

It is worth noting that [25], [26], and [65] along with other works, take into account and try to minimize the fuel consumption needed for the required orbit corrections because it has a large impact on the costs and the lifetime of the mission. Regarding this aspect, electric propulsion (EP) and electromagnetic forces are two interesting fields of research. The EP has higher fuel efficiency than chemical alternatives, in other words, less fuel and propellant storage is required. For this reason, EP is more suitable for small satellites. An interesting overview of the EP methods for small satellites is in [66], while a 1U CubeSat in-orbit experiment with EP is presented in [67]. On the other hand, the use of electromagnetic forces is the most promising technology for fuel-free formations. An interesting section regarding the so-called non-contact forces is in [20], while the patent in [9] envisions a swarm system where electromagnetic coils generate movements to change the relative distance between satellites and magnetorquers generate rotations around the satellite center. Another challenge related to the FF is the creation of the required geometry in space. A solution for free-flying swarms could be the stacking of the satellites in one or multiple satellite deployers. The deployer gives satellites the different initial conditions needed to assure collision-free trajectories while the propulsion capability of each satellite is responsible for the required small orbit corrections. A satellite deployer for CubeSats based on electromagnetic forces is presented in [68].

Despite the challenges, the free-flying swarm also provides opportunities. Firstly, this kind of formation could be reconfigurable in space. A free-flying swarm can adapt its half power beam width according to the requirements of the entire constellation. Less inter-element distance, resulting in a higher HPBW, can be used when the constellation is deployed with a low number of swarms, while a larger inter-element distance, resulting in a narrower HPBW, can be reconfigured when the constellation grows with additional swarms. Secondly, since the swarm elements do not need to be physically connected, they can be easily arranged in the rocket for the launch. The number and shape of the satellite deployers can also take into account the launch capacity of the rocket.

a: MINIMUM INTER-ELEMENT DISTANCE REQUIREMENTS
As highlighted in Section V-A1, formation flying aspects are crucial for the feasibility of free-flying swarms. It is difficult
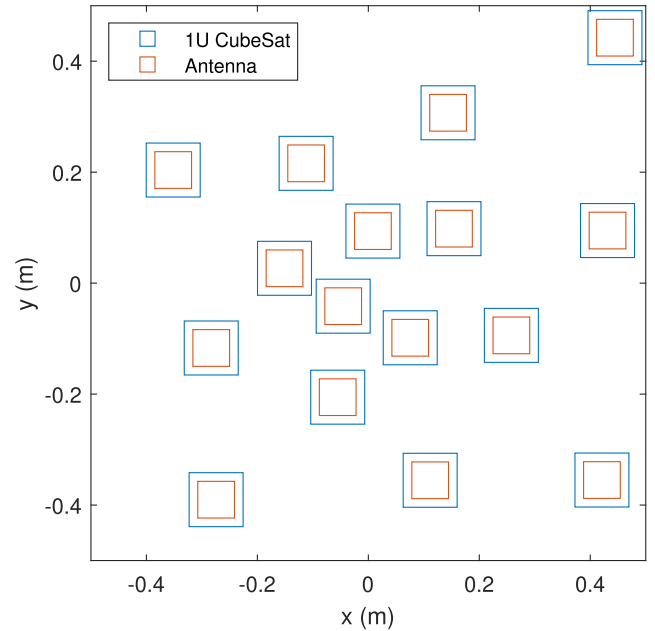

FIGURE 21. ELSA with $N = 100$, $d = 1$ m and $st_c = 0.1$: Zoom on 0.5 m×0.5 m with representation of 1U CubeSats and patch antenna size.

to derive, with the current state-of-the-art, a minimum inter-element distance that can be guaranteed with a formation flying (FF). Nevertheless, promising studies [25], [26], [27] and the growing interest of the scientific community and space agencies [69], [70], [71], [72] could lead to promising developments in the near future.

The URA, ASA and LSA geometries maintain an inter-element distance of approximately 1 m. In contrast, the ELSA geometry, especially with the $st_c = 0.1$ configuration, reduces the inter-element distance up to 0.13 m. Therefore, the feasibility of a swarm with ELSA geometry dictates alternative solutions. Considering the ELSA geometry (Fig. 12), the CubeSat 1U platform and antenna size, the inner part of the structure is shown in Fig. 21.

In this case, possible implementations could be:

- a tethered structure (i.e. physical connection) between the closest satellites;
- a larger satellite incorporating the nearest radiating elements.

Considering the latter alternative, the satellite could be the leader of the formation, already needed to perform other tasks (such as the reference station needed for synchronization and the deployer needed to put the other satellites into orbit).

It is worth noting that multiple values of st_c improve the performance of KPIs compared to the other geometries considered (Fig. 13). Therefore, it is possible to impose a feasibility constraint that defines a minimum value of st_c while maintaining better performance than the uniform spatial density alternative. The constraint must be formulated as a function of distance d and swarm element size.
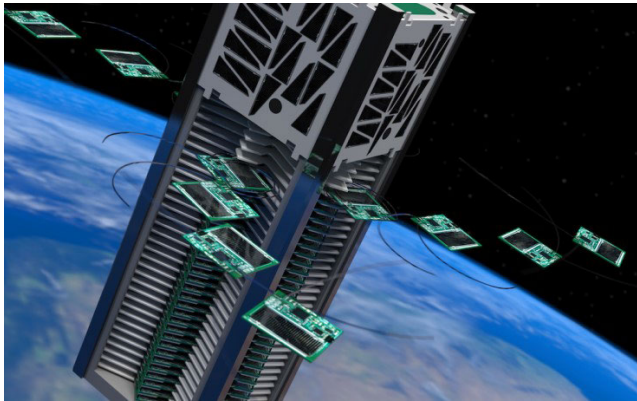
FIGURE 22. Rendering of the KickSat spacecraft and Sprite spacecraft during the deployment phase [73].

FIGURE 23. Example of a tethered swarm with 5 branches and 25 leaves.

2) TETHERED SWARMS

The use of tethers, i.e., a physical connection between the elements, can significantly reduce the complexity of the swarm. Regarding the FF's stability, a tethered structure drastically reduces the impact of the perturbations on the formation. In this case, the orbit corrections are mainly required to keep the whole swarm structure in the desired orbit and not for keeping the formation flying stable. This leads to a reduction of the amount of required propellant as shown in [20] where a tethered swarm with an end-fire array configuration is proposed for a deep-space communication application. In addition, in this case, one larger central satellite of the swarm can be responsible for the correction orbit maneuvers, while the other satellites do not require a propulsion system. Furthermore, the tethered swarm is easier to deploy in space.

Despite the previous advantages, the presence of the tethers complicates the possibility of re-configure the system in space. It also introduces the mechanical challenge to create a deployable structure capable of reducing the size of the swarm for the launch. This challenge is even more important when asymmetric geometries are considered like the LSA and ELSA analyzed in this paper. A large opportunity for the feasibility of the tethered swarm can be the adoption of innovative deployable solutions based on cm-level spacecraft (Fig. 22), like the ones created in the open-source project KickSat [74] used in the NASA KickSat-1 and KickSat-2 missions [75].

a: SPRITE-BASED TETHERED SWARM

The tethered swarm could be realized using a central satellite, similar to the KickSat spacecraft in [73] used in the KickSat mission, designed to unfold multiple branches in space. Each branch of the satellite has multiple leaves. Each leaf of the branch is a very small spacecraft like the Sprite spacecraft in [73] or the SpaceChip first described in [76]. The leaves of one branch are connected through similar tapespring connectors used by the BlueWalker 3. The tapespring connector has two functions: to give mechanical stability to the formation and to provide data connections between the leaves
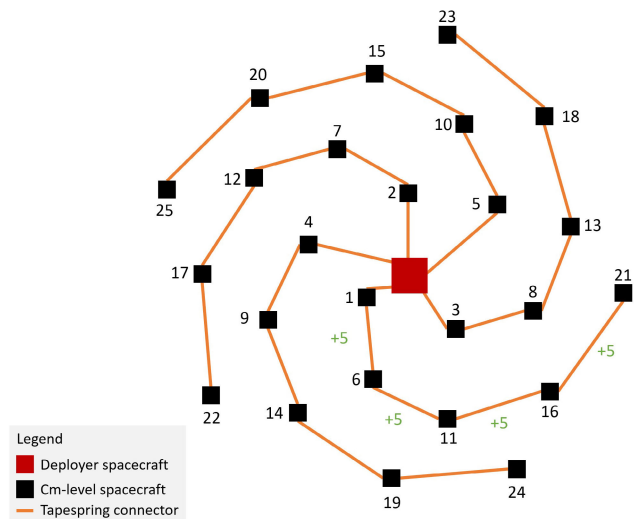
and the central satellite. Fig. 23 shows a schematic tethered swarm with five branches and twenty-five leaves connected to the deployer satellite. The LSA and ELSA architectures analyzed in this paper are particularly suitable for this kind of implementation. They are based on Fermat's spiral geometry with elements placed as described in Sections III-C2 and III-C3. The elements of spiral arrays can be grouped in sets of Fibonacci spirals as explained in the appendix of [13]. An interesting characteristic of this configuration is the possibility to connect the elements of the LSA/ELSA with an arbitrary number of branches. As an example, an LSA geometry with twenty-five elements can be realized with five branches of five elements each, but also with eight branches with three elements each (exception made for one branch with 4 elements). The example in Fig. 23 shows a swarm realized by a leader satellite deployer in the middle of the structure and five branches with five followers each. The first branch is obtained by connecting the followers in positions 1, 6, 11, 16 and 21, the second branch is obtained by connecting the followers in positions 2, 7, 12, 17 and 22 and in the same way it is easy to obtain the other branches. This mathematical property could lead to a practical solution to individually store each branch in the satellite deployer and deploy them individually in space. In this case, the number of branches can be derived from mechanical considerations without altering the geometry of the swarm.

B. FEEDER LINK

A bidirectional link (DL/UL with non-overlapping frequencies) in the Ka/V band between the gateway and the leader of the swarm is a solid option for both free-flying and tethered configurations. In the case of free-flying swarms, an alternative solution could be the direct transmission of the same signal to all the satellites of the swarm but in this case, all the satellites would require an additional transceiver chain in the Ka/V band. An additional reason to have a
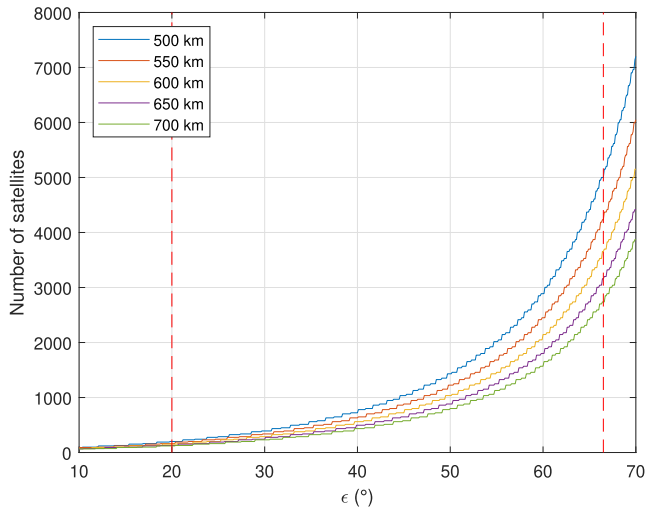
FIGURE 24. Approximated number of satellites required for global coverage with a Walker constellation.

Ka/V dedicated chain in each satellite of the swarm could be the possibility that the gateway transmits different signals already time/phase pre-compensated to shift the processing complexity to the ground segment. In this case, the satellites of the swarm could act only as transparent amplify, convert and forward devices. The drawback of this solution is that the required link capacity of the feeder link grows with the number of satellites of the swarms.

C. UE INITIAL ACCESS
When a service area is only covered by a swarm, an association procedure between the satellite and the UE is required. From a design perspective, firstly, the swarm must have a very small main beam coverage, under 5 km to assure increased frequency reuse. Secondly, the swarm must cover the largest possible area to reduce the number of swarms in the constellation. This means that a swarm needs a large number of possible beams inside the service area. Scanning the service area with the narrow beams, used for data transfer, could result in a long time for the initial access.

The 5G New Radio terrestrial access network uses a beam-sweeping strategy to identify the position of the user inside the base station service area. Broader beams are used to continuously sweep the entire area enabling the UE to start the so-called RACH procedure. After the initial access, the base station knows the position of the user and uses a narrower beam to serve the user.

A similar concept could be applied to the swarm. Preliminary results on the LSA and ELSA geometry, analyzed in Section III-C, have shown that activating only 60 of 100 elements in the center of the swarm can provide a larger beam, with more than 20 km of radius. The broader beams could sweep the service area of the satellite with less time and start the RACH procedure with the UE. To further reduce the initial access time, the historical values of the traffic location

patterns could be used by artificial intelligence algorithms to optimize the beam sweeping sequence.

D. CONSTELLATION OF SWARMS
Before concluding this article, it is necessary to clarify one important aspect. Although the proposed swarm-based antenna is composed of a multitude of small satellites, e.g., 100 as in the simulations, its goal is to replace a single conventional satellite. Therefore, a swarm of satellites in LEO experiences the same conditions as a single conventional satellite. Comparing a LEO satellite with a satellite in higher orbits there are several differences, such as:

- a reduced latency, between 30 and 50 ms (about 8 times less than a MEO satellite and about 35 times less than a GEO satellite);
- a lower propagation loss and a higher Doppler shift;
- a reduced field of view (FoV);
- an increased orbital speed of about 7.5 km/s;
- a reduced orbital period, between 90 and 110 min.

Notably, considering the reduced field of view of the single satellite and the relative motion of the satellite concerning Earth, a constellation of swarms is required to achieve global coverage.

1) TOTAL NUMBER OF SWARMS
The total number of satellites mainly depends on the minimum elevation angle that the constellation aims to guarantee. The elevation angle ϵ is the vertical angle formed between the earth's surface and the line of sight direction between the UE and the swarm (Fig. 2). Considering a high minimum elevation angle in constellation design reduces the service area (coverage) of each satellite, which implies a larger constellation. Simulations suggest a minimum elevation angle of 5° for practical satellite applications [77], but considering urban areas an elevation angle less than 20° would probably result in a total blockage situation due to the shadowing effect, even for low buildings [78]. 3GPP is considering a target elevation angle of 30° for the current study of the integration of non-terrestrial networks in 5G [79]. Preliminary analyses on the direct connectivity in L/S band carried out in [80], based on the ITU Recommendation [81], suggest a constellation design with a high elevation angle (e.g. $\epsilon > 65°$) to overcome urban shadowing.

A recent article [82] showed interesting information about the plans of two major players in satellite direct-to-cell connectivity. AST SpaceMobile is planning a constellation with about 170 huge satellites at altitudes between 550 and 700 km. Lynk Global is planning a constellation with about 5110 smaller satellites at 500 km.

Fig. 24, based on the simple equations in [10], shows the number of satellites of a Walker constellation when the elevation angle varies from 10° to 70° for different LEO altitudes. It is easy to observe that the planned size of AST's constellation should guarantee a minimum elevation angle of about 20°, while the size of Lynk's constellation should

TABLE 6. AST SpaceMobile and Lynk Global comparison.

Description	Parameter	AST	LINK
Planned constellation size (number of satellites)	N_c	170	5110
Maximum size of individual satellite (m^2)	A_s	128	4
Estimated total constellation area (m^2)	$A_c = A_s \cdot N_c$	21760	20440
Estimated number of antenna elements per satellite	$N_e \approx \left(\frac{\sqrt{A_s}}{\lambda} + 1 \right)^2$	5800	200
Estimated minimum elevation angle (°)	ϵ_{min}	21	66.5

guarantee a minimum elevation angle of about 65° (parameter ϵ_{min} in Table 6).

Thanks to the information in [82], Table 6 presents two simple useful metrics:

- the estimated total constellation area (parameter A_c), calculated in the assumption that all satellites in the constellation have the same size equal to the maximum size (parameter A_s);
- the estimated number of antenna elements (parameter N_e), calculated in the assumption of a square planar array with a uniform inter-element distance equal to $\lambda \approx 0.15$ m ($f_c = 2$ GHz).

Parameter A_c of Table 6 delineates a similar end goal for the two constellations despite the huge differences. Parameter N_e of Table 6 shows that the number of antenna elements per satellite is in the order of thousands in the case of the AST approach and the order of hundreds in the case of the Lynk approach. The latter approach considers a number of radiating elements similar to the target of the swarm-based antenna array derived in this work. Due to this similarity, it is convenient to assume that a constellation of swarms should have a similar constellation size, guaranteeing an elevation angle higher than 65°.

The main advantage of the swarm approach over the conventional approach, with a similar number of antenna elements, would lie in the reduction of the half-power beam width, which in turn would allow for better frequency reuse. In other words, the swarm approach has the potential to increase the total satellite throughput compared to the conventional approach.

Although a constellation with thousands of satellites may be frightening, recent techno-economic analyses [83], [84] suggest a sustainable cost regime, comparable to that of terrestrial competitors, to ensure the participation of mega-satellite constellations in future integrated 6G networks. However, considering the high density of potential users on Earth, this apparently already massive number of satellites may not be sufficient to provide reasonable performance [85]. This explains the plans of some companies for mega constellations with tens of thousands of satellites.
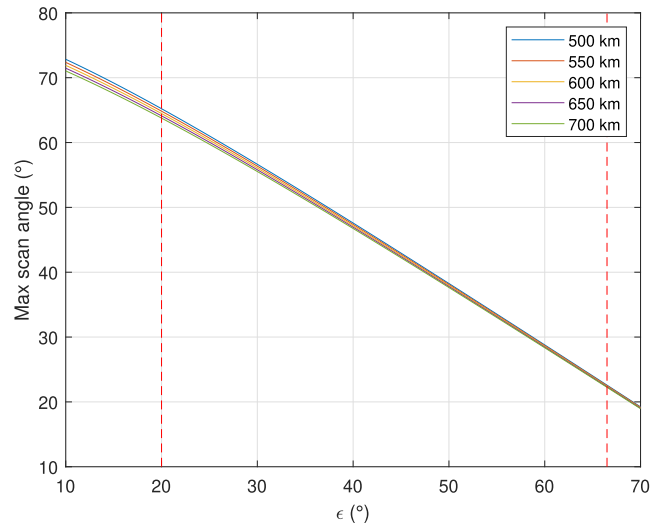
FIGURE 25. Max required scan angle required for a minimum elevation angle.

2) MAXIMUM SCAN ANGLE AREA

Introducing a minimum elevation angle in the constellation design has an important impact on the maximum scan angle area. Using the definition of slant range adjustment [86] and simple geometrical calculations it is possible to relate the elevation angle ϵ with the elevation component of the steering angle θ_s (Fig. 2). Fig. 25 shows the result of this calculation. It is possible to observe that considering a minimum elevation of around 65°, as in this manuscript, the maximum scan angle can be limited to a value below $\theta_s < 25°$.

3) SWARM SERVICE TIME

Another challenge with LEO constellations that aims to provide satellite direct-to-cell connectivity is the handover. Again, the swarm-based antenna array can be considered equivalent to a single conventional satellite.

In the assumption of earth-fixed cells (EFC), where the satellite continuously adjusts the beam direction to fix the beam (or cell) to a specific location on Earth, typical service time values for a LEO satellite range from 100 s to 250 s considering a minimum elevation angle of 10° [87].

In the assumption of earth-moving cells (EMC), where the satellite beam pointing direction is fixed and thus the beam footprint is moving on Earth, the system has to deal with inter-satellite handover and intra-satellite handover (between beams from the same satellite). In this case, the analysis in [88] shows a beam service time below 10 s.

LEO constellations must cope with frequent handovers. The maximization of the service time, i.e., the minimization of the handover rate is an important research aspect in future integrated 6G networks.

VI. CONCLUSION

This work describes the use of satellite swarms for the direct-to-cell connectivity use case. The swarm approach has been

used for other applications but its use for communication and especially for direct connectivity is mostly unexplored. The creation of a large virtual aperture in space with a smaller number of swarm elements promises benefits in terms of performance and costs. The increased distance between the elements generates the known phenomenon of the grating lobes when common planar array geometries are used. For this reason, the geometry of the swarm is studied to mitigate the problem. The paper shows that the logarithmic spiral array (LSA) and the proposed enhanced LSA (ELSA) mitigate the grating lobe problem.

Although the achieved results are encouraging, other challenges need to be faced. For this reason, the paper addresses the main research directions for the success of the swarm approach. In addition, important system design aspects are analyzed and several opportunities are highlighted. In particular, it is shown that swarms in tethered configurations and with spiral geometries can benefit from innovative deployable structures, cm-level spacecraft and particular mathematical properties that can facilitate their implementation.

In conclusion, the designed solution closes the link with a common user terminal, uses a limited number of satellites and reduces the size of the main beam by managing the distance between elements. There is the possibility that multiple swarms with a limited service area could outperform conventional phased array solutions in terms of performance and cost. Further research efforts are needed to bring the swarm approach to a higher level of technology readiness.

ACKNOWLEDGMENT

REFERENCES

[1] *Apple to Debut iPhone With Emergency Messaging Enabled by Globalstar Satellites.* Accessed: Sep. 8, 2022. [Online]. Available: https://www.satellitetoday.com/telecom/2022/09/07/apple-to-debutiphone-with-emergency-messaging-enabled-by-globalstar-satellites/

[2] (Sep. 2022). *The First Phone maker to Add Satellite Texting to Its Devices is…Huawei.* Accessed: Sep. 14, 2022. [Online]. Available: https://www.theverge.com/2022/9/6/23339717/huawei-mate-50-pro-satellite-text-china-beidou

[3] (Apr. 2022). *Lynk Launches Birst Commercial-Ready Cell-Tower-in-Spaceb Telecoms.Com.* Accessed: Sep. 8, 2022. [Online]. Available: https://telecoms.com/514594/lynk-launches-first-commercial-ready-cell-tower-in-space/

[4] B. Duan, Y. Zhang, and J. Du, *Large Deployable Satellite Antennas: Design Theory, Methods and Applications* (Springer Tracts in Mechanical Engineering). Singapore: Springer, 2020, doi: 10.1007/978-981-15-6033-0.

[5] *Large Deployable Reflector Subsystems.* Accessed: Aug. 22, 2022. [Online]. Available: https://www.hps-gmbh.com/en/portfolio/subsystems/deployable-antennas-lea/

[6] *SpaceX Starlink Satellites to Beam Service Straight to Smartphones.* Accessed: Aug. 26, 2022. [Online]. Available: https://www.space.com/spacex-starlink-direct-service-smartphones-t-mobile

[7] *AST SpaceMobile Announces Summer Launch Date of BlueWalker 3 for Direct-to-Cell Phone Connectivity Testing AST Science.* Accessed: Jul. 20, 2022. [Online]. Available: https://ast-science.com/2022/06/13/bluewalker-3-launch-date/

[8] (2022). *AST SpaceMobile Announces Multi-Launch Agreement With SpaceX for Planned Direct-to-Cell Phone Connectivity.* [Online]. Available: https://www.businesswire.com/news/home/20220309005369/en/AST-SpaceMobile-Announces-Multi-Launch-Agreement-With-SpaceX-for-Planned-Direct-to-Cell-Phone-Connectivity

[9] A. Avellan and S. Sriram, "System and method for high throughput fractionated satellites (HTFS) for direct connectivity to and from end user devices and terminals using flight formations of small or very small satellites," U.S. Patent 9 973 266 B1, May 15, 2018.

[10] N. Saeed, A. Elzanaty, H. Almorad, H. Dahrouj, T. Y. Al-Naffouri, and M.-S. Alouini, "CubeSat communications: Recent advances and future challenges," *IEEE Commun. Surveys Tuts.*, vol. 22, no. 3, pp. 1839–1862, 3rd Quart., 2020.

[11] F. Y. Hadaegh, S.-J. Chung, and H. M. Manohara, "On development of 100-gram-class spacecraft for swarm applications," *IEEE Syst. J.*, vol. 10, no. 2, pp. 673–684, Jun. 2016.

[12] A. Ishimaru, "Theory of unequally-spaced arrays," *IRE Trans. Antennas Propag.*, vol. 10, no. 6, pp. 691–702, Nov. 1962.

[13] M. C. Viganó, G. Toso, G. Caille, C. Mangenot, and I. E. Lager, "Sunflower array antenna with adjustable density taper," *Int. J. Antennas Propag.*, vol. 2009, pp. 1–10, Jan. 2009. [Online]. Available: http://www.hindawi.com/journals/ijap/2009/624035/

[14] Y. V. Krivosheev, A. V. Shishlov, and V. V. Denisenko, "Grating lobe suppression in aperiodic phased array antennas composed of periodic subarrays with large element spacing," *IEEE Trans. Antennas Propag.*, vol. 57, no. 1, pp. 76–85, Feb. 2015.

[15] L. Piattella, R. M. Rossi, and I. Russo, "The vertigo array for grating lobe reduction," in *Proc. IEEE Int. Symp. Antennas Propag. USNC/URSI Nat. Radio Sci. Meeting*, Jul. 2017, pp. 1583–1584.

[16] L. Tenuti, P. Rocca, M. Salucci, G. Gottardi, and A. Massa, "Innovative optimization-based design of UWB planar arrays for grating lobes reduction," in *Proc. IEEE Int. Symp. Antennas Propag. USNC/URSI Nat. Radio Sci. Meeting*, Jul. 2017, pp. 2017–2018.

[17] H. Zhang, Y. Liu, W. Zhang, and J. Zhang, "Research on grating lobe suppression of aperiodic array with large spacing," in *Proc. Int. Conf. Microw. Millim. Wave Technol. (ICMMT)*, May 2021, pp. 1–3.

[18] P. P. Sundaramoorthy, E. Gill, and C. J. M. Verhoeven, "Systematic identification of applications for a cluster of Femto-satellites," in *Proc. 61st Int. Astron. Congr.*, Oct. 2010, pp. 1–5. [Online]. Available: http://resolver.tudelft.nl/uuid:b471eea7-5261-4dbf-b388-d410cbde28a5

[19] D. P. Scharf, F. Y. Hadaegh, and S. R. Ploen, "A survey of spacecraft formation flying guidance and control. Part II: Control," in *Proc. Amer. Control Conf.*, vol. 4, Jun./Jul. 2004, pp. 2976–2985.

[20] G. Liu and S. Zhang, "A survey on formation control of small satellites," *Proc. IEEE*, vol. 106, no. 3, pp. 440–457, Mar. 2018.

[21] G. B. Sholomitsky, O. F. Prilutsky, and V. G. Rodin, "Infra-red space interferometer," in *Proc. 28th Int. Astron. Fed. Congr.*, Prague, Czech, 1977, Paper IAF-77-68.

[22] S. Bandyopadhyay, G. P. Subramanian, R. Foust, D. Morgan, S.-J. Chung, and F. Hadaegh, "A review of impending small satellite formation flying missions," in *Proc. 53rd AIAA Aerosp. Sci. Meeting*, Jan. 2015, p. 1623.

[23] S. Bandyopadhyay, R. Foust, G. P. Subramanian, S.-J. Chung, and F. Y. Hadaegh, "Review of formation flying and constellation missions using nanosatellites," *J. Spacecraft Rockets*, vol. 53, no. 3, pp. 567–578, 2016.

[24] K. Alremeithi, J. Miranda Dias, and G. de Masi, "Realization of pattern formation for micro-satellite swarms without a centralized coordination," in *Proc. IEEE Int. Symp. Robotic Sensors Environ. (ROSE)*, Nov. 2022, pp. 01–07.

[25] R. Mazouz, M. Quadrelli, and R. Beauchamp, "Dynamics and optimal control for free-flight and tethered arrays in low Earth orbit," in *Proc. IEEE Aerosp. Conf.*, Mar. 2021, pp. 1–20.

[26] M. Lutzner, T. Jagdhuber, A. Camps, H. Park, M. Peichl, R. Forstner, and M. Jirousek, "Orbit design for a satellite swarm-based motion induced synthetic aperture radiometer (MISAR) in low-Earth orbit for Earth observation applications," *IEEE Trans. Geosci. Remote Sens.*, vol. 60, 2022, Art. no. 1002116.

[27] M. B. Quadrelli, R. Hodges, V. Vilnrotter, S. Bandyopadhyay, F. Tassi, and S. Bevilacqua, "Distributed swarm antenna arrays for deep space applications," in *Proc. IEEE Aerosp. Conf.*, Mar. 2019, pp. 1–15.

[28] M. Y. Abdelsadek, G. K. Kurt, and H. Yanikomeroglu, "Distributed massive MIMO for LEO satellite networks," *IEEE Open J. Commun. Soc.*, vol. 3, pp. 2162–2177, 2022.

[29] R. Deng, B. Di, and L. Song, "Ultra-dense LEO satellite based formation flying," *IEEE Trans. Commun.*, vol. 69, no. 5, pp. 3091–3105, May 2021.

[30] M. Roper, B. Matthiesen, D. Wubben, P. Popovski, and A. Dekorsy, "Beamspace MIMO for satellite swarms," in *Proc. IEEE Wireless Commun. Netw. Conf. (WCNC)*, Austin, TX, USA, Apr. 2022, pp. 1307–1312.

[31] P.-D. Arapoglou, S. Cioni, E. Re, and A. Ginesi, "Direct access to 5G new radio user equipment from NGSO satellites in millimeter waves," in *Proc. 10th Adv. Satell. Multimedia Syst. Conf. 16th Signal Process. Space Commun. Workshop (ASMS/SPSC)*, Oct. 2020, pp. 1–8.

[32] T. Delamotte, M. G. Schraml, R. T. Schwarz, K.-U. Storek, and A. Knopp, "Multi-antenna-enabled 6G satellite systems: Roadmap, challenges and opportunities," in *Proc. WSA 25th Int. ITG Workshop Smart Antennas*, Nov. 2021, pp. 1–6.

[33] G. Bacci, R. de Gaudenzi, M. Luise, L. Sanguinetti, and E. Sebastiani, "Formation-of-arrays multi-satellite high-gain spaceborne antenna for (B)5G communications," in *Proc. 27th Ka Broadband Commun. Conf. (Ka) 39th Int. Commun. Satell. Syst. Conf. (ICSSC)*, Oct. 2022, p. 7.

[34] H. L. Van Trees, *Detection, Estimation, and Modulation Theory. 4: Optimum Array Processing*. New York, NY, USA: Wiley, 2002.

[35] C. A. Balanis, *Antenna Theory: Analysis and Design*, 4th ed. Hoboken, NJ, USA: Wiley, 2016.

[36] *CubeSat Products All of Our Modules, Platforms and Structures*. Accessed: Jun. 10, 2022. [Online]. Available: https://www.endurosat.com/products/

[37] *5G; NR; User Equipment (UE) Radio Transmission and Reception; Part 1: Range 1 Standalone*, Standard (TS) 38.101-1, 3GPP, Version 17.6.0 Release 17, 3rd Generation Partnership Project (3GPP), Technical Specification, Aug. 2022.

[38] A. Braun, "Low earth orbit mechanical deployable structure," U.S. Patent 20 200 361 635 A1, Nov. 19, 2020.

[39] *Application for Mobile Satellite Service by Space Exploration Holdings, LLC SAT-MOD-20220725-00074/SATMOD2022072500074*. Accessed: Nov. 5, 2022. [Online]. Available: https://fcc.report/IBFS/SAT-MOD-20220725-00074

[40] W. L. Stutzman and G. A. Thiele, *Antenna Theory Design*, 3rd ed. Hoboken, NJ, USA: Wiley, 2013.

[41] P. Knott, "Design and experimental results of a spherical antenna array for a conformal array demonstrator," in *Proc. 2nd Int. ITG Conf. Antennas*, Mar. 2007, pp. 120–123.

[42] M. B. Protsenko, M. V. Rozhnovskyi, P. Bannykh, O. Kobylinskyi, and A. A. Iaremenko, "Curved antenna array for application to mobile communication systems," in *Proc. 9th Int. Conf. Antenna Theory Techn.*, Sep. 2013, pp. 261–263.

[43] K. S. Beenamole, C. A. Sreejith, and G. Shankar, "Studies on conformal antenna arrays placed on cylindrical curved surfaces," in *Proc. Int. Symp. Antennas Propag. (APSYM)*, Dec. 2016, pp. 1–3.

[44] J. D. Pack, "Sensor array for enhanced directivity," U.S. Patent 6 778 148 B1, Aug. 17, 2004.

[45] D. Boeringer, "Phased array including a logarithmic spiral lattice of uniformly spaced radiating and receiving elements," U.S. Patent 6 433 754 B1, Apr. 13, 2002.

[46] S. J. Mazlouman, "Distributed phase shifter array system and method," U.S. Patent 20 180 241 122 A1, Aug. 23, 2018.

[47] K. C. Kerby and J. T. Bernhard, "Sidelobe level and wideband behavior of arrays of random subarrays," *IEEE Trans. Antennas Propag.*, vol. 54, no. 8, pp. 2253–2262, Aug. 2006.

[48] M. Dessouky, H. Sharshar, and Y. Albagory, "A novel tapered beamforming window for uniform concentric circular arrays," *J. Electromagn. Waves Appl.*, vol. 20, no. 14, pp. 2077–2089, Jan. 2006, doi: 10.1163/156939306779322701.

[49] M. Nofal, S. Aljahdali, and Y. Albagory, "Tapered beamforming for concentric ring arrays," *AEU Int. J. Electron. Commun.*, vol. 67, no. 1, pp. 58–63, Jan. 2013. [Online]. Available: https://www.sciencedirect.com/science/article/pii/S1434841112001495

[50] M. Hong and Z.-Q. Luo, "Signal processing and optimal resource allocation for the interference channel," in *Academic Press Library in Signal Processing* (Academic Press Library in Signal Processing), vol. 2, N. D. Sidiropoulos, F. Gini, R. Chellappa, and S. Theodoridis, Eds. Amsterdam, The Netherlands: Elsevier, Jan. 2014, pp. 409–469. [Online]. Available: https://www.sciencedirect.com/science/article/pii/B9780123965004000089

[51] M. Sadek, A. Tarighat, and A. H. Sayed, "A leakage-based precoding scheme for downlink multi-user MIMO channels," *IEEE Trans. Wireless Commun.*, vol. 6, no. 5, pp. 1711–1721, May 2007.

[52] F. Rusek, D. Persson, B. K. Lau, E. G. Larsson, T. L. Marzetta, O. Edfors, and F. Tufvesson, "Scaling up MIMO: Opportunities and challenges with very large arrays," *IEEE Signal Process. Mag.*, vol. 30, no. 1, pp. 40–60, Jan. 2013.

[53] E. G. Larsson, O. Edfors, F. Tufvesson, and T. L. Marzetta, "Massive MIMO for next generation wireless systems," *IEEE Commun. Mag.*, vol. 52, no. 2, pp. 186–195, Feb. 2014.

[54] L. You, K.-X. Li, J. Wang, X. Gao, X.-G. Xia, and B. Ottersten, "Massive MIMO transmission for LEO satellite communications," *IEEE J. Sel. Areas Commun.*, vol. 38, no. 8, pp. 1851–1865, Aug. 2020.

[55] K.-X. Li, L. You, J. Wang, X. Gao, and S. Chatzinotas, "Downlink transmit design for massive MIMO LEO satellite communications," *IEEE Trans. Commun.*, vol. 70, no. 2, pp. 1014–1028, Feb. 2022.

[56] J. A. Nanzer, S. R. Mghabghab, S. M. Ellison, and A. Schlegel, "Distributed phased arrays: Challenges and recent advances," *IEEE Trans. Microw. Theory Techn.*, vol. 69, no. 11, pp. 4893–4907, Nov. 2021.

[57] R. Mudumbai, D. R. B. Iii, U. Madhow, and H. V. Poor, "Distributed transmit beamforming: Challenges and recent progress," *IEEE Commun. Mag.*, vol. 47, no. 2, pp. 102–110, Feb. 2009.

[58] G. P. Martin and K. M. Minear, "System and method for widely-spaced coherent transmit arraying using a remote receiver," U.S. Patent 10 270 506 B2, Apr. 23, 2019. [Online]. Available: https://patents.google.com/patent/US10270506B2/en

[59] J. A. Nanzer, R. L. Schmid, T. M. Comberiate, and J. E. Hodkin, "Open-loop coherent distributed arrays," *IEEE Trans. Microw. Theory Techn.*, vol. 65, no. 5, pp. 1662–1672, May 2017.

[60] N. Luo and G. R. Lachapelle, "Relative positioning of multiple moving platforms using GPS," *IEEE Trans. Aerosp. Electron. Syst.*, vol. 39, no. 3, pp. 936–948, Jul. 2003.

[61] P. P. Sundaramoorthy, E. Gill, and C. J. M. Verhoeven, "Enhancing ground communication of distributed space systems," *Acta Astronautica*, vol. 84, pp. 15–23, Mar. 2013. [Online]. Available: https://www.sciencedirect.com/science/article/pii/S0094576512004109

[62] V. Vilnrotter, "Power spectrum of uplink array signals with random phase and delay errors," in *Proc. IEEE Aerosp. Conf.*, Mar. 2012, pp. 1–12.

[63] C. Craeye and D. González-Ovejero, "A review on array mutual coupling analysis," *Radio Sci.*, vol. 46, no. 2, pp. 1–25, Apr. 2011.

[64] H. J. Visser, *Array and Phased Array Antenna Basics*. Chichester, U.K.: Wiley, 2005.

[65] D. Morgan, S.-J. Chung, L. Blackmore, B. Acikmese, D. Bayard, and F. Y. Hadaegh, "Swarm-keeping strategies for spacecraft under J2 and atmospheric drag perturbations," *J. Guid., Control, Dyn.*, vol. 35, no. 5, pp. 1492–1506, Sep. 2012, doi: 10.2514/1.55705.

[66] D. ObReilly, G. Herdrich, and D. F. Kavanagh, "Electric propulsion methods for small satellites: A review," *Aerosp.*, vol. 8, no. 1, p. 22, 2021. [Online]. Available: https://www.mdpi.com/2226-4310/8/1/22

[67] A. Kramer, P. Bangert, and K. Schilling, "UWE-4: First electric propulsion on a 1U CubeSat—In-Orbit experiments and characterization," *Aerospace*, vol. 7, no. 7, p. 98, Jul. 2020. [Online]. Available: https://www.mdpi.com/2226-4310/7/7/98

[68] Y. Zhao, H. Yue, X. Mu, X. Yang, and F. Yang, "Design and analysis of a new deployer for the in orbit release of multiple stacked CubeSats," *Remote Sens.*, vol. 14, no. 17, p. 4205, Aug. 2022. [Online]. Available: https://www.mdpi.com/2072-4292/14/17/4205

[69] M. G. Di, M. Lawn, and R. Bevilacqua, "Survey on guidance navigation and control requirements for spacecraft formation-flying missions," *J. Guid. Control Dyn.*, vol. 41, no. 3, pp. 581–602, 2018.

[70] L. Hall. *What is Starling*. Accessed: Feb. 2, 2023. [Online]. Available: http://www.nasa.gov/directorates/spacetech/smallspacecraft/starling

[71] H. Sanchez, D. Mcintosh, H. Cannon, C. Pires, J. Sullivan, and S. Dâ, "Starling1: Swarm technology demonstration," in *Proc. 32nd Annu. AIAA/USU Conf. Small Satell.*, Aug. 2018, pp. 1–9.

[72] *Join the Hive: Send Your Ideas for CubeSat Swarms*. Accessed: Feb. 2, 2023. [Online]. Available: https://www.esa.int/EnablingSupport/PreparingfortheFuture/DiscoveryandPreparation/Jointhehivesendyourideasfor CubeSatswarms

[73] Z. R. Manchester, "Centimeter-scale spacecraft: Design, fabrication, and deployment," Ph.D. dissertation, Aerosp. Eng., Fac. Graduate School Cornell Univ., Ithaca, NY, USA, Aug. 2015. [Online]. Available: https://hdl.handle.net/1813/41055

[74] *KickSat*. Accessed: Nov. 3, 2022. [Online]. Available: https://kicksat.github.io/

[75] F. Tavares. (May 2019). *What is KickSat-2*. Accessed: Nov. 3, 2022. [Online]. Available: http://www.nasa.gov/ames/kicksat

[76] D. J. Barnhart, T. Vladimirova, and M. N. Sweeting, "Very-small-satellite design for distributed space missions," *J. Spacecraft Rockets*, vol. 44, no. 6, pp. 1294–1306, Nov. 2007, doi: 10.2514/1.28678.

[77] R. K. Ahmed and H. Ibrahim Hamd, "Elevation angle influence in geostationary and non-geostationary satellite system," in *Proc. Int. Conf. Adv. Sci. Eng. (ICOASE)*, Oct. 2018, pp. 212–215.

[78] S. Hornillo-Mellado, R. Martín-Clemente, and V. Baena-Lecuyer, "Prediction of satellite shadowing in smart cities with application to IoT," *Sensors*, vol. 20, no. 2, p. 475, Jan. 2020.

[79] *Solutions for NR to Support Non-Terrestrial Networks (NTN)*, Standard (TR) 38.821 V16.0.0, 3rd Generation Partnership Project (3GPP), 3GPP, Tech. Rep., Dec. 2019.

[80] ESA Conference Bureau. (Oct. 2021). *SPACE2CONNECT21 Direct access to Handheld Devices V 1 Daniel Arapoglou*. [Online]. Available: https://www.youtube.com/watch?v=DnOsZDTTMTk

[81] *Propagation Data Required for the Design Systems in the Land Mobile-Satellite Service*, document Recommendation P.681-11, International Telecommunication Union (ITU), Aug. 2019.

[82] *Your Cellphone Will Be a Satphone*. Accessed: Feb. 3, 2023. [Online]. Available: https://spectrum.ieee.org/satellite-cellphone

[83] K. T. Li, C. A. Hofmann, F. VC6lk, and A. Knopp, "Techno-economic design aspects of satellite mega-constellations for 6G services," in *Proc. IEEE 94th Veh. Technol. Conf. (VTC-Fall)*, Sep. 2021, pp. 1–6.

[84] K. T. Li, C. A. Hofmann, H. Reder, and A. Knopp, "A techno-economic assessment and tradespace exploration of low earth orbit mega-constellations," *IEEE Commun. Mag.*, vol. 61, no. 2, pp. 24–30, Feb. 2023.

[85] O. B. Osoro and E. J. Oughton, "A techno-economic framework for satellite networks applied to low Earth orbit constellations: Assessing starlink, OneWeb and kuiper," *IEEE Access*, vol. 9, pp. 141611–141625, 2021.

[86] B. R. Elbert, *The Satellite Communication Applications Handbook* (Artech House Space Technology and Applications Library), 2nd ed. Boston, MA, USA: Artech House, 2004.

[87] J. S. Baik and J.-H. Kim, "Analysis of the Earth fixed beam duration in the LEO," in *Proc. Int. Conf. Inf. Netw. (ICOIN)*, Jan. 2021, pp. 477–479.

[88] E. Juan, M. Lauridsen, J. Wigard, and P. Mogensen, "Handover solutions for 5G low-Earth orbit satellite networks," *IEEE Access*, vol. 10, pp. 93309–93325, 2022.

THOMAS DELAMOTTE (Member, IEEE) received the Ph.D. degree (Hons.) in telecommunications from the University of the Bundeswehr Munich, in 2019. He is currently a Research Fellow with the Department of Electrical Engineering and Information Technology, University of the Bundeswehr Munich, where he leads the Research Group Digital Satellite Payloads and Satellite Monitoring. He is involved in several projects funded by the German Aerospace Center (DLR). His research interests include the application of advanced signal processing techniques and waveform designs for next-generation satellite systems. His doctoral work on MIMO feeder links has been awarded the TESAT Spacecom Science Award and the VDE Bayern Award.

DIEGO TUZI (Graduate Student Member, IEEE) received the integrated M.Sc. degree in telecommunication engineering from the University of L'Aquila, the Polytechnic University of Milan, and the University of Cassino and Southern Lazio, in 2021. He is currently pursuing the Ph.D. degree with the University of the Bundeswehr Munich. During his studies, he worked in the telecommunication sector for different private companies. Since 2022, he has been a Research Fellow with the University of the Bundeswehr Munich. His research interests include wireless communications, nonterrestrial networks, and future unified networks. He is a member of the Italian Association of Engineers and the Italian Association of Journalists.

ANDREAS KNOPP (Senior Member, IEEE) received the Ph.D. degree (Hons.) in radio communications from the University of the Bundeswehr Munich, in 2008. Since 2014, he has been a Full Professor of signal processing with the Institute of Information Technology, University of the Bundeswehr Munich, Germany, where he coordinates the Germany's largest SpaceCom Laboratory and experimental satellite ground station, the Munich Center for Space Communications. Before taking up the faculty position, he gained expertise as a Communications Engineer and a Satellite Program Manager. He is an Entrepreneur and the Co-Founder of two start-up companies implementing his research. His current research interests include satellite network integration and waveform design for 6G, digital satellite payloads, secure/antijam communications, and low-power mMTC. He is an Advisor to the German MoD and a member of the Expert Group on radio systems in the German Engineers Association VDE/ITG and AFCEA.

● ● ●